Cloud-System Resolving Models: Status and Prospects

Wei-Kuo Tao[1] and Mitch Moncrieff[2]

[1] *Laboratory for Atmospheres*
NASA/Goddard Space Flight Center
Greenbelt, MD 20771

[2]*NCAR*
P. O. Box 3000
Boulder, CO 80307-3000

Submitted to Reviews of Geophysics

Corresponding author address: Dr. Wei-Kuo Tao, Mesoscale Atmospheric Processes Branch, Code 613.1, NASA GSFC, Greenbelt, MD 20771
E-mail: tao@agnes.gsfc.nasa.gov

ABSTRACT

Cloud-system resolving models (CRM), which are based on the nonhydrostatic equations of motion and typically have a grid-spacing of about a kilometer, originated as cloud-process models in the early 1970s. This paper reviews the status and prospects of CRMs across a wide range of issues, such as microphysics and precipitation; interaction between clouds and radiation; Becuasue the effects of boundary-layer and surface-processes on cloud systems. Since CRMs resolve organized convection, tropical waves and the large-scale circulation, there is prospect for several advances in both basic knowledge of scale-interaction requisite to parameterizing mesoscale processes in climate models. In superparameterization, CRMs represent convection explicitly replacing many of the assumptions necessary in contemporary parameterization. Global CRMs have been run on an experimental basis, giving prospect of a new generation climate weather prediction in a decade and climate models due course. CRMs play a major role in the retrievals of surface-rain and latent heating from satellite measurements. Finally, enormous wide dynamic range of CRM simulations presents new challenges for model validation against observations.

1. Introduction

The global hydrological cycle is central to understanding and predicting the weather-climate system, where precipitation physics and moist physical processes in general are major challenges. Approximately two-thirds of the global precipitation occurs in the Tropics, where organized precipitating systems account for a large percentage of rainfall (Nesbitt et al. 2006). Accompanying latent heating accounts for about three-quarters of the total heat energy for the Earth's atmosphere (Riehl and Simpson 1979). The vertical distribution of latent heating strongly affects the large-scale tropical circulation, such as the 30-60-day intraseasonal oscillation (Hartmann *et al.* 1984; Sui and Lau 1988), as well as the global circulation. Fresh water provided by tropical rainfall affects the state of the upper-ocean and ocean-atmosphere interaction. Tropical convection affects midlatitude weather and climate through planetary wave teleconnection, notably in association with El Niño Southern Oscillation (ENSO). Variability in the global circulation can cause prolonged droughts and floods which impact the biosphere, agriculture and humankind. Improved knowledge of the mechanisms responsible for the distribution, variability, and effects of precipitating convective systems is requisite to our knowledge of the global energy and water cycle.

A foremost challenge lies in the accurate parameterization of precipitating cloud systems in global models, a problem of nonlinear interaction among microphysical scales (10^{-3} - 10^{-1} m; seconds-to-minutes), mesoscales (10^{4}- 10^{5} m; hours-to-days) and the large-scale environment. Since mesoscale convective organization is contrary to the assumption of not scale-separation assumed by contemporary parameterizations, new approaches are required. The role of cloud-radiation interaction in weather, climate and hydrological systems is another major challenge. The comprehension required to advance in these areas is formidable. Basically, this is why clouds and radiation is a priority of the Global Change Research Program (GCRP) and the Global Energy and Water Cycle Experiment (GEWEX) inaugurated the GEWEX Cloud System Study (GCSS). In acknowledgement of their emerging importance, cloud ensemble models (CEM), also known as cloud-resolving models (CRM) and cloud-system resolving models (CSRM), were selected as the approach

of choice by GCSS in the early 1990s (GCSS Science Plan 1993; Moncrieff et al. 1997). In this paper we will use the terms CEM, CRM and CSRM interchangeably.

The fine spatial resolution of CRMs (compared to global models) enables explicit interaction among clouds, radiation, precipitation, and surface processes means CRMs are flexible tools for moist processes and scale-interaction research. Collaborative studies conducted by the GCSS and the Department of Energy Atmospheric Radiation Measurement (DOE/ARM) show that CRMs are superior to single-column models (SCMs) wherein physical processes are parameterized (Randall et al. 2003a). Observationally verified CRMs provide a physical basis for not only improving for a range of parameterizations global models but also cloud microphysical parameterizations for CRMs.

Table 1 shows selected highlights CRMs for the past four decades. The earliest kind of cloud model, the one-dimensional (1D) entraining bubble or plume simply represents the lateral entrainment of environmental air. This model was used extensively in cloud-seeding research (Simpson *et al.* 1965, 1967) and is still as the transport module in convective parameterizations. Two-dimensional (2D) cloud models represent cloud development and interactions with the near-environment (Ogura and Phillips 1962). The 1970's witnessed the development of three-dimensional (3D) cloud models with grid-lengths of about a kilometer (Steiner 1973; Wilhelmson 1974; Miller and Pearce 1974; Sommeria 1976; Klemp and Wilhelmson 1978a; Cotton and Tripoli, 1978; Schlesinger 1978; and Clark 1979). The effects of model geometry (i.e., slab-symmetric *vs* axi-symmetric; two-dimensional *vs* three-dimensional) on cloud life-cycles were examined (e.g., Soong and Ogura 1973). Other early studies include the simulation of midlatitude supercells (e.g., Klemp and Wilhelmson 1978b; Wilhelmson and Klemp, 1978) and squall systems (e.g., Moncrieff and Green 1972; Moncrieff and Miller 1976).

Subsequent to GATE[1], cloud ensemble models[2] were used to examine the collective effects of clouds and interaction with the environment and thereby improve cumulus parameterizations (i.e., Soong and Tao 1980; Tao and Soong 1986; Lipps and Helmer 1986;

[1] The Global Atmospheric Research Programme (GARP) Atlantic Tropical Experiment that took place in 1974.

Tao *et al.* 1987; and many others). The challenging quest of improving parameterization continues to this day. Other studies include the effects of ice-processes, radiative processes, on precipitating systems and wind-shear on convective organization (e.g., Thorpe et al. 1980, 1982; Moncrieff 1981; Nakajima and Matsuno 1988; Rotunno *et al.* 1988; Fovell and Ogura 1988; Tao and Simpson 1989; Redelsperger and Sommeria 1986; Lafore et al. 1988; Redelsperger and Lafore 1988; Lafore and Moncrieff 1988; Tao 1995, among others).

In the 1990's, advancing computer power enabled CRMs to examine the large-scale effects of cloud systems and investigate the dynamical basis of multi-scale convective organization (e.g., Grabowski et al. 1998; Wu et al. 1998; Tripoli and Cotton 1989); cloud-chemistry interaction (see review by Thompson *et al.* 1997); idealized climate variability (e.g., Held *et al.* 1993; Lau *et al.* 1993, 1994; Sui *et al.* 1994; Tao *et al.* 1999; and Fig. 1); orographic effects on snowfall (i.e., Saito *et al.* 1996); surface processes (i.e., Lynn *et al.* 1998; Wang *et al.* 2003; Zeng *et al.* 2007); and the development of retrieval algorithms for satellite rainfall (see review by Simpson *et al.* 1996) and latent heating (see review by Tao *et al.* 2006).

Datasets on precipitating convection accumulated from radar, instrumented aircraft, satellites, and rawinsondes deployed in field campaigns during the past generation, (e.g., GATE, TOGA COARE, SCSMEX, KWAJEX, DOE/ARM[3] among others) show the ubiquity of tropical oceanic mesoscale convective systems. A prevalent cloud-system type consists of deep cumulonimbus convection embedded in leading/trailing stratiform regions (e.g., Houze et al. 1980, Zipser 1977; Houze and Betts 198*; Houze 2004). Datasets on precipitating convection accumulated from radar, instrumented aircraft, satellites, and rawinsondes deployed in field campaigns during the past generation, (e.g., GATE, TOGA COARE, SCSMEX, KWAJEX, DOE/ARM[4] among others) show the ubiquity of tropical oceanic mesoscale convective systems. A prevalent type of convective organization of deep

---

[2] Cloud ensemble models allow several convective clouds to develop simultaneously, typically using cyclic lateral boundary conditions.

[3]TOGA COARE for Tropical Oceans Global Atmosphere (TOGA) - Coupled Ocean Atmosphere Response Experiment (COARE); SCSMEX for South China Sea Monsoon Experiment; KWAJEX for Kwajalein Experiment; and the DOE-ARM for Department of Energy-Atmospheric Radiation Measurement.

[4]TOGA COARE for Tropical Oceans Global Atmosphere (TOGA) - Coupled Ocean Atmosphere Response Experiment (COARE); SCSMEX for South China Sea Monsoon Experiment; KWAJEX for Kwajalein Experiment; and the DOE-ARM for Department of Energy-Atmospheric Radiation Measurement.

cumulonimbus convection embedded in leading/trailing stratiform regions, namely mesoscale convective systems, MCS (e.g., Houze et al. 1980, Zipser 1977; Houze and Betts 1982; Houze 2004).

CRMs represent subgrid-scale processes more completely than large-scale models, largely because physical processes are coupled to dynamics at the cloud scale: i) spectral-bin microphysical processes which represent cloud aerosol-chemistry interactions; ii) cloud-

radiation interaction; iii) turbulence; and iv) atmosphere-surface models simulate the water and energy cycles. Over the past four decades, CRM integration times have extended from hours to months, and the number of grid points from less than 1000 to about 100 million. Crucial moist mesoscale dynamical processes and their large-scale effects are represented explicitly in 10,000 km computational domains in two spatial dimensions (i.e., Peng *et al.* 2001; Grabowski and Moncrieff 2001) and 1,000 x 1,000 km^2 domains in three dimensions (Yoshizaki *et al.* 2004; Saito *et al.* 2006). Prototype global cloud-system resolving models exist (Miura et al 2007).

	Highlights
1960's	Loading, Buoyancy and Entrainment
1970's	Slab- vs Axis-symmetric Model Cloud Seeding Cloud Dynamics & Warm rain
1980's	Ensemble of Clouds - Cumulus Parameterization Cloud interactions and Mergers Ice Processes Super Cell Dynamics Squall Line Convective and Stratiform Interactions Wind Shear and Cool Pool Gravity Wave and Density Current Cloud Radiation Interaction
1990's	2D vs 3D Cloud-Radiation Quasi-Equilibrium – Climate Variation Implications Cloud Transport and Chemistry Diurnal Variation of Precipitation GEWEX Cloud System Study (GCSS) Coupled with microwave radiative model for satellite cloud retrieval (TRMM)
2000's	Land and Ocean Processes Multi-scale Interactions Energy and Water Cycle Cloud Aerosol-Chemistry Interactions Cumulus Parameterization Improvements

Table 1: Highlights of cloud model development over the past four decades. [Adapted from Tao and Moncrieff (2003); Tao (2003) and modified in Juang et al. (2007)].

This paper is organized into 11 sections. The physical properties of CRMs are summarized in section 2, followed by the effects of microphysics parameterizations in Section 3. The effects of aerosol, surface-exchange and radiative processes are reviewed in sections 4, 5 and 6, respectively. The diurnal variation of precipitation is summarized in section 7 and satellite applications in section 8. Mesoscale convective organization is the theme of section 9, and future developments in section 10. The paper concludes in section 11.

2. Physical characteristics of CRMs

There are two complementary CRM-based approaches. First, in classical cloud models, which can now be run at very high resolution, a focal issue is convective initiation and process interaction over short periods (hours). When verified against field campaign data, such simulations provide a detailed synthesis of a variety of cloud processes. Second, in the second approach (Soong and Ogura 1980; Soong and Tao 1980; Lipps and Helmer 1986; Tao and Soong 1986; Krueger 1988; and many others) CRMs run at a lower resolution (grid-spacing about 1 km) enable fields of clouds in various stages of their life cycle to interact across a wide dynamic range. When constrained by specified large-scale advection of temperature and moisture (large-scale thermodynamic forcing) derived from observations, these models simulate rainfall, temperature and water vapor distribution with considerable realism (e.g., Tao 2003, Randall *et al.* 2003a and others) and provide a wealth of statistical information usefil parameterization development. The second approach is the basis for global cloud-system resolving models.

Cloud-microphysical processes (nucleation, diffusion growth and collisions between cloud and precipitation particles) are parameterized in CRMs, along with atmospheric turbulence, turbulent exchange at oceanic/terrestrial boundaries, and radiative transfer. Figure 5 shows typical characteristics described briefly below.

a) Dynamical cores

All CRMs are based on the nonhydrostatic equations of motion, which is necessary for a grid-spacing smaller than about 10km. They may be anelastic (Ogura and Phillips 1962),

where sound waves are filtered by neglecting the local time-variation of density in the mass continuity equation, or compressible in which sound waves are retained. Sound waves are meteorologically unimportant, but their fast phase speed (about 300 m/s) severely limit the time step (e.g., a time-step of 2 seconds is needed at 1000m grid-spacing). Klemp and Wilhelmson (1978a) improved computational efficiency by using a semi-implicit time-splitting scheme (equations are split into sound-wave and gravity-wave components). An advantage of the compressible system is that the set of prognostic equations are structurally similar. In contrast, the anelastic approach involves 3D diagnostic (elliptic) pressure equation, although this can be solved efficiently using modern direct (*e.g.*, Fourier Transform) or iterative methods. Ikawa (1988) and Tao and Simpson (1993) showed that compressible and anelastic formulations give similar results, for example, compared to differences that arise due to changing the cloud-microphysics parameterization.

b) Microphysics and precipitation

In CRMs, microphysical and precipitation processes are coupled at cloud-scale and are, therefore, more realistic than in global models. In one-moment bulk microphysical schemes (e.g., Lin *et al.* 1983 and Rutledge and Hobbs 1984) with two-class liquid (cloud water and rain) and three-class ice (cloud ice, snow and graupel/hail), the shapes of non-precipitating (liquid and ice) are assumed to be spherical. The size distributions of the precipitating particles (rain, snow and graupel/hail[5]) follow a three-parameter gamma distribution function such that $N(D) = N_0 D^{\alpha} \exp(-\lambda D)$, where *No* is the intercept parameter, λ the slope of the particle size distribution and α the shape parameter[6]. Only the hydrometeor mass content, proportional to *N(D)*, is predicted. In two-moment bulk schemes (i.e., Murakami 1990; Ikawa *et al.* 1991; Ferrier 1994; Meyers *et al.* 1997; Resiner *et al.* 1998; Walko *et al.* 2000; Morrison *et al.* 2005; and Seifert and Beheng 2005), mass content and the total number concentration are predicted. In the multi-moment bulk microphysical scheme (Milbrandt and Yau 2005), α varies as a function of the mean-mass diameter. The effects of ice processes

[5] Graupel has a low density and a high intercept (i.e., high number concentration). In contrast, hail has a high density and a small intercept. The choice of graupel or hail depends on where the clouds or cloud systems developed (McCumber *et al.* 1991). For tropical clouds, graupel is more representative than hail. For midlatitude clouds, hail is more representative.

on surface rainfall have been quantified identified (Fovell and Ogura 1988; Tao *et al.* 1989; Gao *et al.* 2006a, among others).

Explicit bin-microphysical schemes developed for CRMs examine cirrus development and cloud-aerosol interaction (e.g., Takahashi 1976; Chen and Lamb 1994; Khain *et al.* 2004). Explicit bin-microphysical schemes are based on the stochastic kinetic equations for the size distribution and are functions of water (cloud droplets and raindrops), and ice particles of different habits (i.e., columnar, plate-like, dendrites, snowflakes, graupel and frozen drops). Each type is described in terms of as size-distribution function containing over 30 categories (bins). Nucleation (activation) processes are based on the size-distribution function for cloud condensation nuclei (> 30 size categories). Detailed microphysics calculations are a useful framework for evaluating and improving bulk microphysical schemes. However, the numerous interactions involved in bin-microphysical schemes requires CRM domains to be small and the simulations short.

c) Turbulence

While convective organization involving mesoscale and larger scale dynamics is resolved by CRMs, motion smaller than the grid-scale (sub-grid scale SGS turbulence) have to be parameterized. An ensemble-mean turbulence model represents SGS effects. Typically, a simple k-type (first-order) turbulence closure is used to diagnose the k-coefficient or obtain it from the turbulent kinetic energy (TKE) equation (one-and-a-half order). In the prognostic TKE method, thermodynamic stability, deformation, shear stability, diffusion, dissipation, moist processes and transport of sub-grid energy are included. In the diagnostic method, deformation and stability are used to compute the k-coefficient. The most complex turbulence parameterization used in CRMs is a third-order closure (Krueger 1988). The performance of third-order turbulence closure is similar to the one-and-a-half order TKE approach for deep convective systems. Third-order closure is necessary for simulating shallow cumuli and boundary-layer cumulus (i.e., Cheng and Xu 2006; Cheng *et al.* 2004).

---

[6] For $\alpha = 0$, the equation reduces to an inverse-exponential distribution that was assumed in Lin *et al.* (1983) and Rutledge and Hobbs (1984).

The performance of 2D numerical models in representing 3D convection in the planetary boundary layer (PBL) was discussed in Moeng *et al.* (2004). How well 2D CRMs represent the nonlinear small-scale interactions associated with precipitating convective systems remains an open question, especially in lengthy simulations where feedbacks are not understood well enough.

d) Radiation

Emission and absorption by water vapor and cloud droplets are represented by two-stream longwave radiative transfer schemes in CRMs. Broadband methods for long-wave radiation include the interactions among the gaseous absorption and scattering by clouds, aerosols, air molecules (Rayleigh scattering), and the surface. The treatment of shortwave radiation is also based on broadband approximations. Explicit microphysics and fine horizontal resolution provide relatively realistic cloud optical properties[7] which are crucial for determining the radiation budgets and diurnal variation of precipitation processes. With high spatial resolution, each atmospheric layer is considered either completely cloudy (overcast) or clear. Partial cloudiness is not assumed. See Tao (2003) for a review of mechanisms of cloud-radiation interaction and comparisons among CRMs.

e) Ocean-surface processes

Surface fluxes get complex in the neighborhood of precipitating convection. Two types of surface-flux schemes are typically used. The first is a simple bulk aerodynamic formula where the transfer coefficients for momentum, sensible heat, and latent heat fluxes are functions of wind speed only. The second more complex, but still a bulk approach, based on the Monin-Obukhov similarity theory (Fairall *et al.* 1996). The exchange coefficients in these two bulk flux algorithms differ: i) in the simple bulk aerodynamic formula they increase linearly with wind speed; ii) in the lower wind speed regime (i.e., < 5 m s^{-1}), the exchange coefficients in the second algorithm increase with decreasing wind speed to

[7] Parameterizing cloud optical properties (optical thickness), especially in the presence of the ice phase is still a key issue. Only limited observations are available upon which to base parameterizations for ice clouds.

account for convective exchange at low wind speeds, but decrease if the wind speed exceeds 5 m s^{-1}. In CRMs, sensitivity tests using the firstalgorithm predict much larger surface fluxes of heat and moisture (hence surface rainfall) than those obtained using the second (more complex) algorithm. The boundary layer structure and CAPE in clear and cloudy areas are also sensitive to flux algorithms. Fine vertical resolution is required to properly represent interaction between the ocean and convection (Wang *et al.* 1996).

f) Land-surface processes

Modeling coupled surface-atmospheric processes is crucial to local and regional climatre. Detailed interactive land-surface models of the heterogeneous land surface (soil, vegetation, and land cover/land use) and adjacent near-surface atmosphere coupled to CRMs study the effect of soil moisture distribution and surface fluxes on clouds and rainfall. A land-surface model usually has three elements: i) a soil module that calculates water and heat transfer into at least four water reservoirs (i.e., surface material, a topsoil root layer, a subsoil root layer, and two or more deeper layers that regulate seasonal and inter-annual variability of the soil hydrology; ii) a surface slab of vegetation, litter and other loose material that shades the soil and acts as the source for latent heat flux via transpiration and root water update, intercepts precipitation and dew, and may include plant internal storage; and iii) the surface layer of the atmosphere (up to the lowest grid level of the model), where the fluxes of sensible heat and water vapor are calculated. High-resolution coupled CRM-land surface models investigate how land-surface conditions affect mesoscale circulations (Lynn *et al.* 2001) and the cloud and precipitation processes of both organized convective lines (Baker *et al.* 2001; Mohr *et al.* 2003; Alonge *et al.* 2007) and less-organized convective clouds (Lynn *et al.* 1998; Zeng *et al.* 2007). Quantification of effects of anthropogenic and natural land-cover and land-use change motivated a new generation of land-surface models which include human-induced land-use change (e.g., irrigation, urbanization and agriculture). Vegetation phenology and biogeochemical cycles of carbon and nitrogen which control photosynthesis/and transpiration are included in the newest land-surface models.

3. Effects of microphysical parameterizations

Latent heat is released or absorbed by the atmosphere as a result of phase changes in water (condensation or evaporation of cloud droplets and raindrops, freezing of raindrops, melting of snow and graupel/hail, or the deposition and sublimation of ice particles). Latent heating is the main contributor to the convective available potential energy (CAPE) for precipitating convection. Cloud-microphysics affects the vertical distribution of cloud species and size distributions (i.e., from small cloud water droplets and ice particles, to medium-sized snow, to large precipitating rain drops and graupel/hail), aspects which affect active (i.e., radar reflectivity) and passive (i.e., brightness temperature) remote-sensing measurements. Since precipitation can be in the form of light rainfall, heavy rainfall, snow, or mixed phase, it influences surface properties (i.e., soil moisture, runoff, albedo, emissivity) and the energy and water cycle. Convective transport affects the vertical redistribution of chemical species which, in turn, affects radiative forcing and atmospheric electrification. Figure 6 summarizes key microphysical interactions.

Figure 7 depicts the widely used two-class liquid (cloud water and rain) and three-class ice (cloud ice, snow and graupel/hail) microphysics schemes. Warm-cloud (i.e., ice-free) microphysics assumes a bimodal the population of water particles, consisting of small cloud water droplets whose terminal velocity is negligible compared to vertical velocity of air, and large rain droplets that obey certain size distributions. Condensation, evaporation, and autoconversion/collection processes (from small cloud droplets to large rain droplets) are parameterized. Ice microphysics typically assumes three types of particle: small cloud ice whose terminal velocity is negligible, snow whose terminal velocity is about 1-3 m s^{-1}, and large graupel or hail with faster terminal velocities. Graupel has low density and high intercept (high number concentration) while hail has a high density and a small intercept. Graupel is representative for tropical oceanic convection and hail for midlatitude storms (McCumber *et al.* 1991). More than 25 transfer processes among water vapor, liquid and ice particles are included: growth of ice crystals by riming, the aggregation of ice crystals, the formation of graupel and hail, the growth of graupel and hail by the collection of supercooled rain drops, the shedding of water drops from hail, the rapid growth of ice crystals in the presence of supercooled water, the melting of all forms of ice, deposition and the sublimation of ice. Only large rain droplets, snow and graupel/hail reach ground-level.

Figure 8 emphasizes microphysical and kinematic aspects of precipitation processes in the convective and stratiform regions (Houze 1982, 1989). Ice is generated once growing drops are lofted through the 0 °C level in convective updrafts. Thereafter the ice particles grow by riming as they accrete super-cooled cloud drops forming in the updraft at mid-to-upper levels. Larger particles fall out rapidly as convective rain and smaller particles that fall more slowly (~1 m s^{-1}) are advected through the stratiform region. The detrainment of the snow from the convective cells is how precipitating particles are introduced into the stratiform region of the cloud system. Also the most intense radar bright band and the heaviest stratiform rain at the surface occur where the convectively generated snow particles reach the 0 °C level, after their passage through the stratiform cloud. In this environment of widespread moderate vertical motion, snow particles precipitate and grow by vapor deposition. In the layer between 0 and -12 °C, the particles aggregate into snowflakes and grow by riming. Influx of snow into the stratiform region from the convective cells and growth of snow on passing through the mesoscale updraft contributes to stratiform precipitation. See the reviews of Houze (2004) and Tao (2003) for details.

Figure 9 illustrates the instantaneous CRM-simulated microphysics associated with MCSs observed in the mid-latitude continental PRE-STORM[8] and the tropical oceanic TOGA-COARE field-campaigns, respectively. Evident are: i) condensation heating in the lower to middle troposphere of the convective leading edge of the cloud systems; ii) deposition heating in the upper parts of the convective and stratiform regions; iii) cooling in low-level stratiform regions due to the evaporation of rain; iv) cooling due to melting of precipitation near the freezing-level (550-600 hPa); and v) sublimation cooling adjacent to depositional heating in the stratiform regions. The alternating heating-cooling pattern at upper levels is caused by convectively-generated gravity waves, and are more significant for the mid-latitude case because of the stronger the convective updrafts. Cooling within the stratiform region is larger and deeper in mid-latitudes due to the drier environment. The simulated structures are consistent with observed tropical cloud systems.

a) ***Ice phase***

---

8 PRE-STORM (Preliminary Regional Experiment for STORM-Central) took place in Kansas and Oklahoma during May-Jun85 (Cunning 1986).

Tao and Simpson (1989) showed that the introduction of ice-phase microphysics does not significantly affect the propagation speed of a simulated MCSs, which is dominated by downdrafts and the associated cold outflow. The lifecycle and total precipitation do not differ significantly (see Table 2), nor does the total evaporative cooling in the stratiform and convective regions. Such small differences (< 1 to 2 m s^{-1}) with and without ice-phase processes were reported in Yoshzaki (1986), Nicholls (1987), Fovell and Ogura (1988) and Chen (1991). The main difference concerns the precipitation statistics. Light rain (< 10 mm h^{-1}) accounts for only about 26.5% of the total rain, but it covers 90% of the total rain area for the ice run. By contrast, heavy precipitation (> 30 mm h^{-1}) accounts for a large portion of the total rain, but occupies a very small portion of the total rain area. Without ice-phase microphysics, heavy precipitation is increased significantly and only 12% of the rain is stratiform. The depth of the stratiform cloud is reduced with ice-free microphysics. These results agree with GATE observations (see Table 1 in Tao and Simpson, 1989).

	Total Rain (mm/12h)	Stratiform Portion	Total Rain Area (%)	Stratiform Rain Area (5)
Ice-run	24.9	32.7%	22.3	86.8
Ice-free	23.4	11.5%	8.1	66.1

Table 2: Estimated surface rainfall and rainfall area at the surface. Rain is given in relative units (millimeters per grid point accumulated over a 12 h period). The total rain area is given as a percentage of the total domain area. Stratiform portion and stratiform rain area are given as a percentage of total rain and total rain area, respectively. Adapted from Tao and Simpson (1993).

A 4-class microphysical (4ICE) combines features of 3-class ice (3ICE) schemes by calculating the mixing ratios for both graupel and frozen drops/hail (Ferrier 1994; Ferrier *et al.* 1995). Additional variables include the number concentrations of all ice particles (small ice crystals, snow, graupel and frozen drops), as well as the mixing ratios of liquid water in each of the precipitation ice species during wet growth and melting for purposes of accurate active and passive radiometric calculations. Also included are: i) more accurate calculation of accretion processes, including partitioning the freezing of raindrops as sources of snow, graupel and frozen drops/hail; ii) consideration of rime densities and riming rates in converting between ice species due to rapid cloud water riming; iii) incorporation of new parameterizations of ice nucleation processes, the rime splintering mechanism using laboratory data, and the aircraft

observations of high ice particle concentrations; iv) shedding of liquid water from melting ice and from excessive amounts of water accumulated on super-cooled frozen drops/hail; v) preventing unrealistically large glaciation rates immediately above the freezing-level by explicitly calculating freezing rates of raindrops and freezing rates of liquid water accreted onto super-cooled ice; vi) introducing fall speeds and size distributions for small ice crystals; vii) calculating radar reflectivity of particles with variable size distributions and liquid water coatings from Rayleigh theory; viii) basing conversion of particle number concentrations between hydrometeor species on preserving spectral characteristics of particle distributions rather than conserving their number concentrations (important). A detailed description of these parameterized processes can be found in Ferrier (1994).

For the most part, ice schemes do not significantly affect the organization of cloud systems (Fig. 10). For example, the arc-shape is simulated in agreement with observations (Jorgensen *et al.* 1997). The propagation speeds of the squall system simulated by both schemes are similar (14 m s^{-1}), about 2 m s^{-1} faster than observed. However, ice microphysical parameterizations affect the surface precipitation about 30% less with 4ICE than 3ICE (Table 3). The evolution of stratiform rain during the lifecycle of the squall systems differs in the 4ICE and 3ICE schemes. The 3ICE scheme produced more/less stratiform rain early/later in the simulation because the different hydrometeor profiles. Small ice particles (cloud ice and snow) with slow fall speeds (1 - 3 m s^{-1}) are more dominant in the 4ICE scheme. The 3ICE scheme produces more and larger graupel (with 2 - 5 m s^{-1} fall speeds) in the convective towers, which is transported into the trailing stratiform region of the squall system.

	3ICE	**4ICE**
Rainfall (mm)	**13.38**	**10.06**
Stratiform percentage (%)	**35%**	**35%**

Table 3: Surface rainfall amounts (mm) accumulated over 9 hours for CRM simulated TOGA COARE squall systes using the 3ICE and 4ICE schemes. The percentage of rainfall that was stratiform is also given.

c) *Explicit ice- microphysics*

Explicit bin-microphysical schemes study the impact of the atmospheric aerosol on cirrus and deep convective precipitation (Khain *et al.* 1999)., and are based on stochastic kinetic equations for the size distribution functions of water droplets (cloud droplets and raindrops), and ice particles of different habits (i.e., columnar, plate-like, dendrites, snowflakes, graupel and frozen drops). Each type is described by a size-distribution function containing over 30 categories (bins). Nucleation (activation) processes are also based on the size distribution function for cloud condensation nuclei (also over 30 size categories). The numerous interactions involved in bin-microphysical schemes, require small computational domains are small and short simulations. The explicit approach is a framework for evaluating and improving bulk microphysical schemes.

Figure 11 shows the vertical cross section of simulated observed radar reflectivity for a mature stage of a squall line. Large differences exist between the radar reflectivity structure simulated by the bulk and bin schemes, especially in the stratiform region. Both the size or the stratiform area and stratiform fraction are much larger in the bin simulation (see Table 4). The stratiform region simulated by the bin scheme is homogeneous, with no sign of convective cells. On the other hand, cellular convective structures in the form of high radar reflectivity cores are evident. These cells are remnants of the previous convection cells that propagate rearward and decay. Radar reflectivity observations of the PRE-STORM squall are widely reported (e.g., Smull and Houze 1987a,b; Rutledge et al. 1988; Rutledge and MacGorman 1988; Biggerstaff and Houze 1993).

	Bulk 3ICE microphysical scheme	Spectral-bin microphysical scheme
Rainfall (mm)	64.5	56.9
Startiform (%)	6.6%	19.6%

Table 4: Surface rainfall amounts (mm) accumulated over 12 hours for CRM simulated PRESTORM squall system using the 3ICE bulk and spectral bin microphysical schemes. The percentage of rainfall that was stratiform is also given. Adapted from Li et al. (2008b).

4. *Effects of aerosol*

The effect of aerosols on clouds is an issue for the climate system and the hydrological cycle (Ramanathan et al., 2001), but the processes involved are not well understood. A recent report published by the National Academy of Science states "*The greatest uncertainty about the aerosol climate forcing - indeed, the largest of all the uncertainties about global climate forcing - is probably the indirect effect of aerosols on clouds [NRC, 2001].*" The aerosol effect on clouds is often categorized into the traditional "first indirect (i.e., Twomey)" effect on the cloud droplet sizes for a constant liquid water path [Twomey, 1977] and the "semi-direct" effect on cloud coverage [e.g., Ackerman et al., 2000]. Enhanced aerosol concentrations can also suppress warm-rain processes by producing a narrow droplet spectrum that inhibits collision and coalescence processes [e.g., Squires and Twomey, 1961; Warner and Twomey, 1967; Warner, 1968; Rosenfeld, 1999].

Properties	High CCN (Dirty)	Low CCN (Clean)	References (Observations)
Cloud droplet size distribution	Narrower	Broader	*Rosenfeld and Lensky* [1998], *Rosenfeld* [1999 & 2000], *Rosenfeld et al.* [2001], *Rosenfeld and Woodley* [2000], *Andreae et al.* [2004], *Koren et al.* [2006],
Warm-rain process	Suppressed	Enhanced	*Rosenfeld* [1999 & 2000], *Rosenfeld and Woodley* [2000], *Rosenfeld and Ulbrich* [2003], *Andreae et al.* [2004], *Linn et al.* [2006]
Cold-rain process	Enhanced	Suppressed	*Rosenfeld and Woodley* [2000], Orville et al. [2001], Williams *et al.* [2002], *Andreae et al.* [2004], *Linn et al.* [2006], *Bell et al.* [2007]
Mixed phase region	Deeper	Shallower	*Rosenfeld and Lensky* [1998], Williams *et al.* [2002], *Linn et al.* [2006]
Cloud-top height	Higher	Lower	*Andreae et al.* [2004], *Koren et al.* [2006], *Linn et al.* [2006]
Lightning	Enhanced (downwind side)/higher max flash	Less and lower max flash	*Williams et al.* [2002], *Orville et al.* [2001]

Table 5. Key observational studies identifying the differences in the microphysical properties, cloud characteristics, thermodynamics, and dynamics associated with clouds and cloud systems developed in dirty and clean environments. Adapted from Tao et al. (2007).

The aerosol effect on precipitation processes (the second aerosol indirect effect, Albrecht, 1989) is more complex, especially for mixed-phase convective clouds. Table 5 summarizes observational studies identifying the microphysical properties, cloud characteristics, thermodynamics and dynamics associated with cloud systems from high-aerosol continental environments. For example, atmospheric aerosol concentrations can

influence cloud droplet size distributions, warm-rain process, cold-rain process, cloud-top height, the depth of the mixed phase region, and occurrence of lightning. Hypotheses have been developed to explain the effect of urban regions on convection and precipitation [*van den Heever and Cotton*, 2007 and S*hepherd*, 2005]. Please see Tao *et al.* (2007) for more detailed description on aerosol impact on precipitation.

Figure 12 shows that rain suppression at high CCN concentration (i.e., dirty environment) but only during the first hour of the simulations. Rain reaches the ground early in all the clean cases, in agreement with observations [e.g., Rosenfeld, 1999, 2000]. During the mature stage of the simulations, the effect of increasing the CCN concentration ranges from rain suppression in the PRESTORM case to little effect in the CRYSTAL-FACE case to rain enhancement in the TOGA COARE case. These results suggest that model simulations of the whole life cycle of convective system are needed in order to assess the impact of aerosols on precipitation processes associated with mesoscale convective systems and thunderstorms. These results also show the complexity of aerosol-cloud-precipitation interaction within deep convection.

Table 6 shows the domain-averaged surface rainfall amounts, stratiform percentages, precipitation efficiencies, and ice water path ratios (ice water path divided by the sum of the liquid and ice water paths) for the TOGA COARE, PRESTORM and CRYSTAL-FACE cases under clean and dirty conditions. The precipitation is divided into convective and stratiform components [Tao et al., 1993; Lang et al., 2003]. The convective region includes areas with strong vertical velocities (over 3-5 m s^{-1}) and/or heavy surface rainfall. The stratiform region is simply non-convective. For the PRESTORM case, the dirty scenario produces more stratiform (light) precipitation than does the clean case. It is expected that a high CCN concentration allows for more small cloud droplets and ice particles to form. The lower collection coefficient for smaller cloud and ice particles allows for a larger amount of ice phase particles to be transported into the trailing stratiform region, producing a higher stratiform rain percentage in the dirty case. Aerosols do not have much impact on the straiform percentage for the CRYSTAL-FACE case because of its short life span. The reduction in stratiform rain (or light rain) in the dirty environment for the TOGA COARE case is due to its enhanced convective activity (stronger updrafts).

	TOGA COARE Clean	*TOGA COARE Dirty*	*PRESTORM Clean*	*PRESTORM Dirty*	*CRYSTAL Clean*	*CRYSTAL Dirty*
Averaged Rain (mm/day/grid)	18.0	28.4	38.3	29.1	12.6	11.0
Stratiform (%)	50	17	43	70	43	40

Table 6 Domain-averaged surface rainfall amount (in mm day^{-1}), stratiform percentage (in %) for the TOGA COARE, PRESTORM and CRYSTAL-FACE case under dirty and clean conditions. Note there are 9 hours in the PRESTORM and TOGA COARE simulations, and 5 hours in the CRYSTAL-FACE simulation. Adapted from Tao et al. (2007)

Figure 13 shows the physical processes that cause either enhancement (TOGA COARE) or suppression (PRESTORM) of precipitation in a dirty environment. In the early developing stages, small cloud droplets are produced in both the TOGA COARE and the PRESTORM cases with high CCN. Both cases also show narrower cloud drop size spectra for high CCN (not shown). This result is in good agreement with observations [i. e., *Twomey et al.,* 1984; *Albrecht,* 1989; *Rosenfeld,* 1999]. In this early stage, rain is suppressed for both cases with high CCN, which is also in good agreement with observations [*e.g., Rosenfeld,* 1999, 2000]. The suppression of precipitation in dirty conditions is mainly due to microphysical processes only. Smaller cloud droplets collide/coalesce less efficiently, delaying raindrop formation. These microphysical processes are seemingly very important especially in the early/developing stage of a cloud system.

The modeled low-level evaporative cooling is quite different between the clean and dirty case. Stronger evaporative cooling could enhance the near surface cold-pool strength. When the cold pool interacts with the lower level wind shear, the convergence could become stronger, producing stronger convection for the dirty cases. This can lead to more vigorous precipitation processes and therefore enhanced surface precipitation (positive feedback)[9]. These processes seemingly occur in the TOGA COARE case. In this case, evaporative cooling is more than twice as strong in the lower troposphere for the dirty scenario compared to the clean scenario. More rain reaches the surface after 30 minutes of model integration in

[9] Note that the enhanced precipitation can cause enhanced evaporation that in turn has a positive feedback on the rainfall amounts by triggering additional convection.

the dirty case as compared to the clean case. During this period, more evaporative cooling in the dirty case is already evident from the model results.

Most previous modeling results found that high CCN concentrations coulsuppress precipitation processes [e.g., Khain et al., 2004, 2005; Cheng et al., 2007, Lynn et al., 2005b; Van den Heever et al., 2006; Teller and Levin, 2006; van den Heever and Cotton, 2007]. However, high CCN concentrations could also enhance precipitation processes [*Wang 2005*; *Khain et al.* 2005]. These results show the complexity of aerosol interactions with convection.

5. Effects of surface-exchange

The surface and atmosphere are strongly coupled. Over land, the surface fluxes are coupled to the surface net radiation flux, the vegetation state, and the profiles of temperature and water below the surface and up through the atmospheric planetary boundary layer. These processes at the land-atmosphere interface are strongly influenced by topographic features and the heterogeneous character of the land surface layer. The fluxes of heat and moisture across the interface vary on spatial scales ranging from meters to thousands of kilometers. On the other hand, the western Pacific warm pool is a region of enhanced atmospheric sensitivity to small changes in the ocean temperature (Simpson 1988; the TOGA COARE Science Plan). Modeling these coupled surface-atmospheric processes is crucial to the understanding and simulation of climate system interactions.

a) Ocean-surface fluxes

Observational studies in the western Pacific warm pool region (Bradley *et al.* 1991; Young *et al.* 1992; Fairall *et al.* 1996) show that surface heat and momentum fluxes all have a peak in the convective leading edge due to strong gust winds and colder air temperatures in the convective region. The surface fluxes in the large clear area are much smaller and more uniform than those in the convective region.

Figure 15 shows the rainfall and surface latent heat flux values using the TOGA COARE flux algorithm and the simple bulk aerodynamic method[10]. The different flux algorithms do not effect the organization of the squall system. Both runs also show a large peak in latent heat flux at the leading edge of the convection, about 4-5 times the value in the clear area. This is due to the stronger winds and colder temperature in the cloudy convective region. The 9-hour rainfall total simulated with the TOGA COARE flux algorithm is about 73% of the rainfall amount using the bulk aerodynamic method. Larger surface fluxes cause more rainfall (or precipitation processes). A sensitivity study using the GCE model by Wang *et al.* (2001) indicated that surface fluxes from the large clear area are more influential to the rainfall amount than the fluxes from the disturbed convective area because the moisture supply to the convective system is mainly from the clear area ahead of the convective system. The stratiform amounts between these two runs are very similar (about 35%). Horizontal wind shear has a major effect on convective organization and stratiform rain (see section 6 for more discussion).

Table 7 lists the accumulated domain-normalized surface rainfall amounts as well as horizontally averaged latent and sensible heat fluxes for the disturbed (convective) and undisturbed (cloud-free) areas simulated from three different surface flux formulations [Blackadar Planetary Boundary Layer[11], simple bulk aerodynamic method and TOGA COARE Flux algorithm]. The surface heat fluxes and the surface rainfall are correlated, but the relationship is not linear. Similar amounts of surface precipitation were simulated using the Blackadar surface fluxes and the bulk aerodynamic method, though the fluxes computed from the bulk aerodynamic method are significantly larger than those from the Blackadar method. These features can also be seen in Fig. 16, which shows that the latent heat fluxes from the three flux formulations are quite different, especially along the leading edge of the squall system (gust front region). The latent and sensible heat fluxes in the convective (disturbed) region are larger than those of the non-convective (clear) region due to the gust wind speed, a cool pool near the surface, and drier air from downdrafts associated with the

---

[10] The TOGA COARE bulk flux algorithm was developed and calibrated with the TOGA COARE surface flux data set. Simple bulk aerodynamic methods have been used frequently in CRMs as well as in hurricane models.

[11] The Blackadar PBL (BLK hereafter), which has been widely applied in regional modeling studies associated with convective systems.

convective activity. Additional sensitivity study also indicated that surface fluxes from the large clear area are more influential to the rainfall amount than the fluxes from the disturbed convective area because the moisture supply to the convective system is mainly from the clear area ahead of the convective system.

	Surface Rainfall (mm)	Sensible Heat Fluxes		Latent Heat Fluxes	
		Disturbed	Undisturbed	Disturbed	Undisturbed
COARE Flux	3.4	20.9	8.4	142.2	81.7
Aerodynamic	4.5	31.1	12.9	206.5	127.7
Blackadar	4.2	24.4	10.7	170.8	110.6

Table 7: Estimated surface rainfall at the surface for simulations using different surface flux formations. Also shown the ensemble averaged sensible and latent heat fluxes in the disturbed (convective) and undisturbed (non-convective) regions for simulations using different surface flux formulations. Adapted from Wang et al. (1996).

The results from TOGA COARE flux algorithm are in good agreement with observations (LeMone *et al.* 1995; Young *et al.* 1995). Both Blackadar and simple bulk aerodynamic formulation predicted larger latent and sensible heat fluxes than those from the TOGA COARE flux algorithm. These differences can cause large deviations in the amount of precipitation simulated. A large database gives the TOGA COARE flux algorithm an advantage in the simulation of tropical convective systems. Good agreement in surface fluxes may imply that the modeled wind, temperature, and moisture fields in the lower troposphere are realistic compared to observation (Jorgensen *et al.* 1995).

The convective available potential energy (CAPE, Moncrieff and Miller, 1976) is the integrated potential temperature difference between the moist adiabatic ascent of a surface parcel and the environment. It follows that the surface fluxes affect the value of CAPE. The sensible heat flux is usually small over the ocean and the latent heat flux more important. LeMone (1980) and Trier *et al.* (1995) suggested that the CAPE in clear regions should remain quasi-steady during convection. Only the simulation with the TOGA COARE flux parameterization gives a quasi-steady base state CAPE (see Wang *et al.* 2003 for details).

b) Land-surface fluxes

The land and atmosphere form a highly coupled system. The surface convective fluxes are coupled to the surface net radiation flux, the vegetation state, and the profiles of temperature and water, below the surface and up through the atmospheric planetary boundary layer. These processes at the land-atmosphere interface are influenced in a fundamental way by topographic features and the heterogeneous character of the land surface layer. The fluxes of heat and moisture across the interface vary on spatial scales ranging from meters to thousands of kilometers. In addition, clouds are coupled to the underlying surface, it is interesting to explore how to represent the coupling between clouds and the land surface in GCMs. Highly quality cloud data collected at the DOE ARM SGP (Atmospheric Radiation Measurement - Southern Great Plains) site give an opportunity to evaluate the effect of a land surface on clouds with the aid of a high-resolution CRM

A 20-day CRM simulation was evaluated with ARM observations. High-density ARM EBBR stations provided surface fluxes to the model. The ARM surface fluxes come from the EBBR stations, which use the Bowen ratio to partition the fluxes. There are a total of 14 EBBR stations. A grid of 0.5 x 0.5 degrees was first set up to cover the ARM domain (Fig. 17). In addition to the ARM surface fluxes, the surface fluxes extracted from NASA land information system (LIS, see Kumar *et al.* 2007)[12], a land data assimilation system with 1 km horizontal resolution was used to provide surface fluxes for cloud simulations. This LIS simulates soil moisture (both liquid and frozen), soil temperature, skin temperature, canopy water content, and the energy flux and water flux terms of the surface energy and surface water balances. The land-surface parameters were initialized with 1 km datasets for vegetation and land-sea masks (Hansen *et. al.* 2006). Climatological datasets were ingested in order to initialize other vegetation parameters such as albedo and green vegetation fraction. Soils types were set using the State Soil Geographic Database for State [Soil Survey Staff, Natural Resources Conservation Service, United States Department of Agriculture], which has a 1 km horizontal resolution. Initial soil water and temperature profiles were also assigned according to climatology. A snap shot of the spatial distribution of the LIS surface fluxes is shown in Fig. 18. The horizontally averaged surface fluxes are also shown in the

---

12 The LIS is capable of resolving mesoscale features, including urban areas, lakes, and agricultural fields, and this capability will allow us to study the impact and scaling of such heterogeneity in coupled cloud modeling.

lower part of Fig. 17 in comparison with the ARM surface fluxes. As shown in the figure, the surface fluxes from ARM and LIS are close except that they are different from day 4 to 9.

Figure 19 displays the observed and the modeled (twenty-day) cloud amount for comparison. There is a strong diurnal variation of modeled cloud amount from day 4 to 9 when the ARM surface fluxes are used but not when the LIS fluxes are used. This cloud amount difference coincides with a difference between the ARM and LIS surface fluxes from day 4 to 9 (Fig. 17). This improvement is attributed to the large LIS sensible and small latent heat fluxes from day 4 to 9. The surface relative humidity decreases when the sensible heat flux increases and the latent heat flux decreases, therefore the lifting condensation level increases and, in turn, cloud amount in the lower troposphere decreases. This connection between surface fluxes and the diurnal variation of clouds in the lower troposphere is consistent with the difference in relative humidity in the planetary boundary layer between the two experiments. Evidently it is necessary to properly represent the coupling between clouds and a land surface on a sub-grid scale in GCMs.

When coupled to a complex soil-vegetation land model, CRMs simulate moist convection developing over a heterogeneous landscape and measure the effects of precipitation on soil moisture Lynn *et al.* (1998) examined a sea-breeze-like front observed during CaPE (the Convection and Precipitation Electrification Experiment, over Florida) in a total of 28 two-dimensional CRM simulations. Alternating patches of dry and wet soil and for various profiles of background wind were used. The most intense rainfall occurred along the sea-breeze-like fronts occurring at patch boundaries. The largest/smallest CAPE occurred over the wet/dry patch. The heaviest rainfall maximum did not coincide with the largest CAPE, it occurred along the sea-breeze-like fronts for intermediate values of CAPE. This demonstrates that the initiation of moist convection is strongly affected by the dynamic forcing at fronts associated with landscape-generated mesoscale circulations.

A systematic impact of patch length and background wind on moist convection occurred. Total accumulated rainfall (averaged over simulations with the same patch size but with different background wind profiles) was largest for a patch length of 128 km. While the deposition of rainfall generated a much different distribution of soil moisture after one day of

simulation, this distribution was not in equilibrium. The landscape consisted of wet and dry soil patches (Fig. 20). The suggests the need to account for the triggering of moist convection by land surface heterogeneity in atmospheric models.

6. Effects of radiative processes

A high priority in earth system science is to understand the coupling between radiation processes and cloud dynamics. On the one hand, clouds reflect incoming solar and outgoing long-wave radiation. The Earth Radiation Budget Experiment (ERBE), which provided quantitative estimates of global distributions of cloud-radiative interaction, showed that large (stratiform) anvil clouds reflect a significant amount of short-wave radiation (Ramanathan *et al.* 1989), suggesting that clouds effect an net cooling. On the other hand, radiation can enhance or reduce the cloud activity. Gray and Jacobsen (1977) suggested that differential cooling in cloudy and clear regions can enhance the cloudy region. Long-wave radiation cools the stratiform cloud top but warms the stratiform cloud base (Cox and Griffith 1979), so long-wave radiation can destabilize the stratiform cloud layer. Webster and Stephens (1980) suggested that this destabilization was important for light precipitation region during WMONEX. Stephens (1983) deduced the effects of radiation on the growth and sublimation rates of ice particles. Particle growth (sublimation) is enhanced (suppressed) in a radiative cooled (heated) environments. Radiative cooling could also destabilize the large-scale environment (Dudhia 1989).

Cloud-radiation interaction can impact the diurnal variation of precipitation in the tropics. Thermodynamic and dynamic mechanisms have been proposed. On one hand, Kraus (1963) and Randall *et al.* (1991) suggested that the thermodynamic response of clouds to radiative heating [cloud development is reduced by solar heating and enhanced by IR cooling] is the main mechanism responsible for the diurnal variation of precipitation. On the other hand, Gray and Jacobson (1977) indicated that the large-scale dynamic response to the difference in radiative heating between cloudy and clear regions was the main mechanism. Furthermore, Ramanathan *et al.* (1989) concluded that cooling by cloud activity is more significant than previously estimated and could offset the warming effect caused by human activity (*e.g.,* increase in CO_2). *(The cloud influence is about four times as great as that*

caused by increasing carbon dioxide). Because of the lack of complete theoretical treatment and observation, the coupled cloud-radiation-Greenhouse effect is still poorly understood and needs to be studied further in order to better understand potential climate change.

7. Diurnal variation of precipitation

The diurnal variation of precipitation processes over the tropics is a well-recognized but poorly understood phenomenon. Improved understanding of this diurnal cycle is needed in order to make reliable monthly estimates using twice daily satellite observations (i.e., TRMM and SSM/I). The diurnal cycle of precipitation has been studied using surface rainfall data, radar reflectivity data, and satellite-derived cloudiness and precipitation. For example, observations indicate a diurnal cycle with a nocturnal-early morning precipitation maximum over open oceans and an afternoon-evening maximum over land (Kraus 1963; Gray and Jacobsen 1977; Randall *et al.* 1991 and many others).

CRMs have been used to determine "mechanisms" associated with the diurnal variation of precipitation processes (Sui *et al.* 1998). Figure 21 shows the simulated diurnal variation of surface rainfall obtained from five sensitivity tests. The run that did not allow for the diurnal variation of radiative processes (Run 3) failed to produce a diurnal variation of rainfall. Note that the diurnal variation of rainfall was simulated even when the diurnal variation of SST was not allowed (Run 1). Results suggest that the diurnal variation of sea surface temperature could modulate rainfall processes, but it only may play a secondary role in diurnal variation.

Sui *et al.* (1998) found that modulation of convection by the diurnal change in available water, as a function of temperature was responsible for a maximum in rainfall after midnight. This implies that the increase (decrease) in surface precipitation associated with longwave cooling (solar heating) was due to an increase (decrease) in relative humidity (Fig. 22). A similar conclusion was found by Tao et al. (1996). For more discussions and comparison with observations and with results from other cloud resolving models, see Sui *et al.* (1998), Tao *et al.* (1996) and Tao (2003).

The physical processes responsible for diurnal variation in precipitation differ among CRMs. For example, Xu and Randall (1995) found that nocturnal convection is a direct result of cloud-radiation interactions, in which solar absorption by clouds stabilized the atmosphere. However, their simulated rainfall for non-interactive and interactive radiation were similar. Liu and Moncrieff (1998) performed a 15-day integration similar to Sui *et al.* (1998) and showed that direct interaction of radiation with organized convection was the major process that determined the diurnal variability of rainfall. Their results also indicated that well (less) organized cloud systems can have strong (weak) diurnal variations of rainfall. They advocated a need for ice processes. However, the model set-upsof Sui *et al.* (1998) and Liu and Moncrieff (1998) are different.. In Liu and Moncrieff (1998), the horizontal momentum was relaxed to its initial distribution (strong vertical shear in horizontal wind). On the other hand, the horizontal wind was nudged to time-varying observed values in Sui *et al.* (1998). Consequently, long-lived fast-moving squall lines were simulated in Liu and Moncrieff (1998) over the entire simulation whereas in Sui *et al.* (1998) the cloud systems had different sizes and life cycles. A systematic CRM inter-comparison would be desirable, but not before quality observational data are available for verification and initial conditions.

8. Satellite applications

Precipitation is highly variable in space and time and crudely represented in the global circulation models and climate model, therefore latent heat release and its vertical distribution in these models are oversimplified. The Tropical Rainfall Measuring Mission (TRMM), a joint U.S./Japan space project, has been providing a measurements of rainfall over the global tropics using an inclined low-altitude orbit and a combination of precipitation radar, VIS/IR and microwave radiometers (see Simpson *et al.* 1988, 1996)[13]. A major TRMM objectives is to advance our understanding of the global energy and water cycle by providing *four-dimensional distributions of rainfall and inferred heating* over the globe (Simpson 1988). In help meet this objective, CRM can provide 4D data sets (ice/water

[13] TRMM satellite has been successfully flown over a decade, and provided the spectacular fine-resolution views of cloud-precipitation systems from Visible/Infrared Scanner (VIRS), TRMM Microwave Imager (TMI), and Precipitation Radar (PR) sensors (Simpson *et al.* 1995).

cloud structure and melting level) as testbed for satellite remote-sensing measurements.. Three such applications are presented below.

a) ***Surface rain retrieval algorithms***

The retrieval of rainfall information from satellite passive microwave observations is inherently linked to the microphysical structure and dynamics of the cloud system being observed. Especially with intense convective systems, the four-dimensional relations between surface rainfall, suspended hydrometeors, and the resulting upwelling radiances at various passive microwave frequencies are complex. The problem is compounded because the hydrometeor contents and physical properties of such convective systems are difficult to measure over large spatial scale and continuous time period. The vertical structure of the cloud parameters (hydrometeors) drives radiative transfer calculations that determine upwelling radiance at the top of the atmosphere. CRMs provide synthetic data sets (i.e., ice-water distribution) for developing the surface rainfall retrieval (Adler *et al.* 1991; Smith *et al.* 1992, 1994a; Kummerow *et al.* 1996; Panegrossi *et al.* 1998; Olson *et at.* 2006).

There are two basic types of passive microwave rainfall retrieval algorithms, histogram and profiling algorithm. The histogram technique uses the emission properties of the 10, 19 and 37 GHz channel to obtain monthly rainfalls (Wilheit *et al.* 1991) over ocean areas. In this technique, the observed emission signal is related to rainfall in each channel via relationships obtained from radiative transfer calculations through modeled raining atmospheres. Since each microwave frequency has a distinct dynamic range, the algorithms being developed will blend the rainfall distributions obtained from each of the channels into a single distribution, from which rainfall accumulations are inferred. By taking advantage of the known statistical distributions of rainfall rates, this technique can thus compensate for the poor sampling of a polar orbiting radiometer, especially at the high rainfall rates. It is possible that CRM can also provide statistical distributions of rainfall rates over wide range of cloud-types which are occurred in different geographic location.

The second method, profiling algorithm, makes use of the fact that weighting functions for various frequencies peak at different levels within a rainy atmosphere in order to determine the vertical structure of hydrometeors. Because the total information that needs

to be retrieved far exceeds the number of independent observations, however, these algorithms generally make use of CRM to provide first guess profiles (Simpson *et al.* 1988; Adler et al. 1991; Smith et al. 1991). For example, a self-consistent iterative technique (Kummerow *et al.* 1989) has been developed to retrieve hydrometeor distributions from multichannel passive microwave observations. The technique relies on a large set of CRM simulated distinct cloud structures to simulate T_Bs. Consistency between observed and simulated T_Bs is then used to select the cloud structure that best fits the rainfall scene in question. For each structure, radiative transfer calculations that account for multiple scattering through the Eddington approximation are used to calculate the T_Bs of different microwave frequencies.

b) Retrieved of latent heating

These are calculated over a wide range of surface rainfall rates, surface temperatures and emissivities, and vertically integrated cloud (non precipitating) water contents. A set of linear regression coefficients relating each of these parameters as a function of T_B in each of the microwave channels is determined separately over different rain rate intervals using piece wise-linear statistics. Recently, this profile algorithm is improved by using the precipitating profile derived from TRMM combined radar-radiometer algorithm (see Fig. 23). Because of the observed brightness temperature are consistent with those derived from radiative transfer model embedded in the combined radar-radiometer algorithm, the precipitation-brightness temperature data base is considered to be physically consistent.

The TRMM satellite provides a much-needed measurement of rainfall as well as an estimate of the four-dimensional structure of latent (diabatic) heating over the global Tropics. TRMM, however, is unable to directly measure LH profiles, so they have to be determined indirectly from the application of physically based models to TRMM precipitation measurements. The general approach is to apply models, ranging in complexity from simple profile shapes to CRMs, to TRMM PR and/or TMI data (see a review by Tao *et al.* 2006).

Five TRMM LH algorithms have been developed, compared, validated, and applied in the past decade. Table 8 denotes the type(s) of TRMM algorithm(s) that each of the

algorithms use for data input used to generate their associated heating product(s), the mainstream algorithm heating product(s) themselves, and the salient reference(s) describing the designs of each of the heating algorithms. The CSH, GPROF, and SLH algorithms require the full complement of cloud model data generated by a CRM (or CRMs). Recently, a comprehensive intercomparison between the different LH algorithms applied to various common TRMM data sets has been conducted. The emphasis has been on understanding strengths and weaknesses of different methods and underlying assumptions -- an indispensable process for guiding generational upgrades in algorithm philosophy and design. Seven separate datasets: four field experiment cases[14]: SCSMEX, TRMM-LBA, KWAJEX, and DOE-ARM; two tropical cyclone cases: Atlantic Hurricane Bonnie and Pacific Typhoon Jelewat; and one large-scale regional case: a tropical ocean domain are considered for the inter-comparison project. In conducting the validation analyses for four field experiment cases, a set of quantities involving heating terms diagnostically estimated from the sounding network and retrieved from the satellite algorithms are compared. This consists of the following: (1) temporal and horizontal domain-averaged LH/Q_1/Q_1-Q_R vertical structures, (2) altitude of maximum heating, (3) convective and stratiform heating vertical structures, (4) horizontal distribution of LH at different altitudes, and (5) contoured frequency with altitude diagrams (CFADs) of heating.

	TRMM Data Needed	Heating Products	Key References in Algorithm description	Algorithm Developers
CSH (Convective-Stratiform Heating)	PR, TMI, PR-TMI	Q_1, LH	Tao *et al.* (1993; 2000; 2001)	W.-K. Tao & S. E. Lang
SLH (Spectral Latent Heating)	PR	LH, Q_1-Q_R	Shige *et al.* (2004; 2007)	S. Shige & Y. N. Takayabu
TRAIN (Trained radiometer algorithm)	TMI (PR training)	Q_1-Q_R, LH	Grecu and Olson (2006), Olson *et al.* (2006)	M. Grecu & W. Olson
HH (Hydrometeor Heating)	PR-TMI	LH	Yang *et al.* (1999; 2006)	E. A. Smith & Y. Song
PRH (Precipitation Radar Heating)	PR	LH	Satoh and Noda (2001)	S. Satoh & A. Noda

[14] SCSMEX *(South China Sea Monsoon Experiment)* took place over South China Sea (SESA and NESA stands for south and north enhanced sounding arrays, respectively). TRMM-LBA *(Large Scale Biosphere-Atmosphere Experiment in Amazonia)* took place in Rondonia, Brazil. KWAJEX *(TRMM Kwajalein Experiment)* took place around Kwajalein Atoll, Republic of Marshall Islands. DOE-ARM *(Department of Energy-Atmospheric Radiation Measurement)* Program supports cloud-radiation experiments in Oklahoma at Southern Great Plains-Cloud and Radiation Test Bed (SGP-CART) site.

Table 8: Summary of the five LH algorithms participating in the 1st TRMM LH intercomparison / validation project (see Tao et al. 2006 for further details and salient references). Data inputs, retrieved products, and salient references included. Note conventional relationship between Q_1 (apparent heat source), LH, and Q_R (radiative heating) is expressed by Q_1-Q_R = LH + EHT, where the final term represents eddy heat transport by clouds (noting that vertically integrated EHT is zero, i.e., it provides no explicit influence on surface rainfall).

Figure 24 illustrates 5-year averaged Q1 at three different altitudes (2, 5 and 8 km) over the global Tropics from the CSH algorithm based upon the PR rainfall product. Note that the upper and lower altitudes are typical for ice-mixed and warm rain microphysics responsible to levels of the maximum heating. The horizontal distribution of the estimated Q1 structure at middle and upper troposphere is similar to the pattern of surface rainfall. For example, well defined ITCZs in the east and central Pacific and Atlantic Oceans, a well-defined SPCZ in the central-southern Pacific Ocean, and broad areas of precipitation events spread over the continental regions are all evident. Also, strong heating release in the upper troposphere (5°C day^{-1} and greater) is associated with heavier surface precipitation. Heating in the upper troposphere over the Pacific and Indian Oceans covers a much broader area than the heating over Africa, South America, and Atlantic. The large scale heating distributions (i.e., differential latent heating) between continents and oceans and within continents and oceans by themselves are capable of altering the ambient horizontal gradients in the temperature fields that then can feedback to the general circulation. An interesting feature observed in Fig. 24 is the relatively weaker heating at the 2 km level, in comparison to the upper-tropospheric levels, throughout the regions exhibiting strongest rain rates. However, there is more distinct land-sea contrast. Shallow heating is occurred almost exclusive over ocean and nor much over land (except in the Maritime continent). The importance of shallow convection through moistens the lower troposphere, prior to large-scale organized convective systems has been observed and recognized.

These LH products represent a valuable new source of data to the research community. These data products enable new insights and investigation of the complexities of convective life cycles, the diabatic heating controls and feedbacks of meso-synoptic circulations and their forecasts. The distributions of rainfall and inferred heating can be used

to advance understanding of the global energy and water cycle (Morita *et al.* 2006). Three global models, Florida State University (FSU), the NASA Goddard Space Flight Center (GSFC), and NASA Goddard Institute of Space Science (GISS) are currently using TRMM-based LH data sets to improve cumulus parameterization schemes while at the same time addressing physical shortcomings with the schemes (Rajendran *et al.* 2004; Chen *et al.* 2007; Hou and Zhang 2007).

c) CRMs coupled to radar models

As in the single-wavelength TRMM PR, there are a number of error sources that must be understood before assessing the quality of the information derived from the retrievals (Iguchi *et al.* 2000). Because the radar signals attenuated, a path-attenuation constraint has been shown to be useful in bounding the errors in the rain rate estimates. Nevertheless, estimates of path-attenuation via the surface reference technique are themselves limited in accuracy by the natural variability of the surface scattering properties (Meneghini *et al.* 2004). Other factors that will affect the accuracy of the retrievals include: attenuation effects caused by cloud liquid water and atmospheric gases; uncertainties in the scattering properties of mixed phase hydrometeors; and effects of surface clutter on near-surface rain rate estimates. Added to these are instrument-related errors such as the variability in the radar return power from a finite number of samples, radar calibration errors, and beam filling effects.

Detailed study of these error sources will be possible with a radar simulation program using input data from CRMs (References?). For example, the CRM simulated four-dimensional synthetic cloud data set provided insight into the behavior of the snow, rain and surface returns as a function of incidence angle and rain intensity thereby providing an assessment of the sensitivity and dynamic range of the PR instrument. The results also provided an understanding of the effects of beam filling and attenuation from various atmospheric constituents and their effects on rain rate retrieval accuracy. Apart from the 'deterministic' calculations from the storm and surface model, the simulated radar returns were used to test the initial set of PR algorithms. These calculations proved useful in debugging the computer codes, testing the validity of some of the algorithm assumptions, and comparing the performance of competing algorithms.

9. Mesoscale convective organization

Satellite imagery shows that atmospheric convection frequently occurs in lines, clusters, and clumps on various spatio-temporal scales. Field-campaigns and satellite measurements show that cumulus convection often forms long-lasting coherent systems (mesoscale convective organization) hundreds of times the scale of individual cumulus. MCSs which consist of heavily precipitating cumulonimbus embedded in mesoscale regions of lighter stratiform precipitation are highly organized. TRMM precipitation radar, microwave imager and visible infrared scanner measurements show a clear link between MCSs and rainfall. Figure 3 shows MCSs to be the dominant heavy rain producers in the tropics and subtropics. MCSs provide more than 50% of rainfall in most regions with average annual rainfall exceeding 3 mm/day and up to 90% of rainfall over certain continental areas (i.e., La Plata Basin). Differences between land and ocean MCS morphology are associated with regionally distinctive rainfall regimes.

Typically, MCSs occur in sheared environments. Over continents they occur downstream of mountain chains and in association with the midlatitude and subtropical jet streams (e.g., Laing and Fritsch 1997, Carbone et al. 2002). Over tropical oceans MCSs tend to be associated with wave disturbances wherein the shear tends to be larger than average for the tropics (e.g., Straub and Kiladis 2002; Kiladis et al. 2003; Haertel and Kiladis 2004). MCSs redistribute the primary greenhouse gases (e.g., water vapor and carbon dioxide) and, most importantly, sensible and latent heat. The unique vertical transport of horizontal momentum associated with MCSs (see later) directly affects the large-scale atmospheric circulation and also impacts atmosphere-ocean interaction.

Tropical field campaigns have revealed a wealth of knowledge about MCS structure over a period of four decades. In the Zipser (1977) conceptualization of a tropical oceanic MCS with a leading-line/trailing stratiform structure (Fig. 4), sub-cloud air ascends in

convective updrafts, which are weakened through entraining low equivalent-potential-temperature environmental air. Evaporating precipitation and precipitation loading generate convective downdrafts. The airflow is three-dimensional (3D): updrafts and downdrafts bypass each other in a "crossover zone". In the conceptual model of Houze et al. (1980), the MCS is populated by convective cells ranging in size from shallow non-precipitating cells to medium-sized precipitating cells to deep precipitating cells (Fig 3). Each cell contains an updraft and a downdraft. The raining stratiform region contains a mesoscale updraft between level Z_M and Z_{TM} and a mesoscale downdraft between Z_D and Z_M. Figures 4 and 5 have features in common with tropical oceanic convective systems observed in numerous field campaigns. The physical properties of MCSs established during the 1970s and 1980s are summarized in several text books, for example, Ludlam (1980), Cotton and Anthes (1989), Houze (1993), Smith (1997) and the review paper of Houze (2004).

a) MCS dynamics

In organized convection dynamics, the bulk effects of latent heating and how it interacts with environmental shear are the key properties to approximate. The above field-campaign conceptualizations provide a conceptual justification for modeling organized MCS dynaics in terms of a steady, propagating, three-branch system depicted in Fig. 3a. This strictly two-dimensonal model consists of: i) a tilted propagating jump-like updraft; ii) an overturning updraft; ii) an overturning downdraft (Moncrieff 1981, 1992, 1997 and papers cited therein). This dynamical model has been verified against observations (LeMone and Moncrieff 1993). The backward tilt of the propagating is important. With this morphology, precipitation falls into the subsaturated environment where it can maintain downdrafts through the effects of water loading and evaporative cooling. Moreover, the backward tilt has important implications for convective momentum transport (see Section ?). A forward-tilted updraft would be intrinsically unsteady since water loading and evaporation would disrupt the updraft and limit the downdraft.

The Lagrangian timescale of an MCS is typically hours so the dominant thermodynamic processes affecting the value of convective available potential energy

(CAPE), are latent heating and evaporative cooling which is easily approximated. However, in addition to CAPE, two sources of dynamic energy are available to organized convection. First, -level inflow (typically ~ 10-20 m/s) that stems from environmental shear and the propagation speed of the MCS assures that mean-flow kinetic energy, $AKE = \frac{1}{2}(U_0 - c)^2$, is available for the two organized updraft branches, and the propagating branch especially. Second, work done by the cross-system pressure gradient ($AWP = \Delta p / \rho$) is available by virtue of the hydraulic work-energy (Bernoulli) principle. These three quantities define two fundamental variables: the convective Richardson number $R = CAPE/AKE$ (Moncrieff and Green 1972), and the 'Bernoulli number' $E = AWP/AKE$ (Moncrieff and Miller 1976).

Importantly, steady propagation occurs only in limited subsets of *R-E* space. The simplest dynamical model of the thee-branch organixaztion, namely the Moncrieff (1992) archetypal model, conclusively shows that steady convective overturning can when CAPE is zero (Fig. 3b). The value of *E,* in the archetypal model lies in the range $-\frac{8}{9} \le E \le 1$, identifies three specific regimes of convective organization: i) density currrent-like systems (E = -8/9), which resembles the classical Benjamin (1968) density current, except its fractional depth is 2/3 instead of ½. This morphology results the non-stagnant density current in the archetypal model (Moncrieff and So 1989); ii) symmetric systems (E=0), which resembles observed MCS structure; and iii) hydraulic jump-like systems (E=1), which resembles a special type of organizatin, the narrow cold-frontal rainband (Carbone 19**, Moncrieff 19**). The latter solution shows that MCSs and density currents are within the same class of organized convection and their origin is the aforementioned hydraulic work-energy principle (i.e., E).

The above arguments are based on strictly 2D dynamics. Replacing the 2D jump updraft by a 3D propagating circulation thatoverturns in the plane *transverse* to the direction of travel results in an archetypal 3D MCS that containis the aforemetioned observed "crossover zone" (see Moncrieff and Miller 1976) .

b) Convective organization and regime transitions simulated by CRMs

The CAPE and shear vary systematically over periods of a few days in tropical easterly waves that are embedded within the InterTropical Convergence Zone (ITCZ). Snapshots from a 7-day CRM simulation shows transitions among three convective regimes (non-squall cloud cluster, squall cluster, and scattered convection) that occurred in concert with the variation of CAPE and shear across the easterly wave. The squall cluster, which occurs for moderate CAPE and strong shear, is a numerical realization of the relationship among convective organization, CAPE and shear encapsulated in the above dynamical model as R and E. This shows that CRMs realistically simulate observed precipitating convection provided when forced by large-scale variables. This justifies the use of CRMs as a convective parameterization (see Section ??).

c) Representing convective organization in global model

Compared to the copious process studies of MCS from field-campaign m cloud-resolving modeling and dynamical models (see Section 4) have been conducted during the past few decades (Section 40, little has been done to represent convective organization in weather and climate models. The multiscale convective organization and its large-scale effects are only beginning to be quantified. The modern development of lengthy integrations of CRMs with large-scale and even global computational domains providing useful insight.

On timescales exceeding about 10 days (about the timescale of the atmospheric water cycle) the redistribition mass, moisture, heat and momentum by precipitating convection and interactions involving radiation, the land surface, and ocean surface are fundametal to the large-scale atmospheric circulation. The large-scale efects of mesoscale convective orgainzation is a case in point. We show below that backward tilted systems of the MCS-type is a preferred mode of convective organization in large-domain CRMs.

Inertial-gravity waves of low vertical wavenumber ('bore waves') impart the effects of convective heating to the far-field ar important in the formation of large-scale convective clustering (e.g., Nicholls et al. 1991, Mapes 1993, Liu and Moncrieff 2004, Tulich et al. 2007). The vertically gravest (first-baroclinic) mode stabilizes the near-environment by the compensating subsidence response to deep heating but its influence is limited by the fast

phase speed (~50 m/s). The second-baroclinic mode propagates more slowly (~20 m/s) and produces low-level lifting that constructively destabilizes the near-environment and promotes new convection. The decreased convective inhibition promotes convective clustering. Lane and Reeder (2001) showed this process occurs in the neighborhood of individual cumulonimbus. The rotation of the Earth confines convectively-generated gravity waves to the Rossby radius of deformation, which led Liu and Moncrieff (2004) to reason that the largest cloud clusters should be preferred in equatorial regions (infinite Rossby radius).

CRMs integrated for tintraseasonal time scales provide insight into the evolution of large-scale convective coherence, and its association with convectively-generated inertial-gravity waves. Grabowski and Moncrieff (2001) showed that MCS-like systems evolve from an initially motionless and thermodynamically uniform initial state (Fig. 5). The large-scale organization consists of backward-tilted westward-propagating systems embedded an eastward-propagating large-scale cloud envelope. The backward-tilted MCS redistribute horizontal momentum in the vertical and generate vertical shear. This constituted positive dynamical feedback since shear is important in convective organization, recalling section 4. Apart from their horizontal wavelength, the large-scale envelopes in Fig. 6 resemble eastward-traveling superclusters in the MJO (see following section).

a) Madden-Julian oscillation

The Madden-Julian oscillation (MJO; Madden and Julian 1972) is a remarkable spatio-tempotal hierarchy of convective organization: cumulonimbus (~1-10 km, hour), meso-convective clusters (~100-500 km, day), synoptic-scale superclusters (~1000-2000 km, week), and the planetary-scale cloud envelope (~10000 km) which identifies the MJO. Difficulties global models experience with MJOs (ECMWF 2003; Lin et al. 2006, Moncrieff et al. 2007) are often attributed to deficiencies in convective parameterization. Superparameterization (an approach in which atmospheric convection is represented explicitly by CRMs in contrast to contemporary parameterization) circumvents this problem to a considerable degree. Note, however, with a grid-spacing of a few kilometers the CRMs presently used in superparameterization do not resolve cumulonimbus convection.

The multiscale convective organization in atmospheric Kelevin waves is broadly similar to that in the MJO. A case study of a convectively coupled Kelvin wave in the eastern Pacific intertropical convergence zone by Straub and Kiladis (2002) shows a large-scale convective envelope (zonal scale ~1000–2000 km) propagating eastward at 15 m s^{-1} along the ITCZ. Within this envelope are smaller-scale, westward-moving convective elements, with zonal scales a few hundred kilometers. The convectively coupled Kelvin wave strongly controls the convective regime. As the Kelvin wave approaches from the west, convection deepens, progressing from isolated, shallow cumuli to organized deep convection and stratiform precipitation: organized propagating convective systems.

Analogs of the MJO and convectively coupled waves occur in CRMs. In the Grabowski (2001) aquaplanet simulation, an MJO-like system evolved after about 40 days of integration stating from a horizontally homogeneous and motionless initial state (Fig. 6). The MJO regime was preceded by slower-moving and higher-wavenumber systems and extensive large-scale wave activity.

b) Dynamical models of large-scale tropical convective organization

Paralleling the dynamical models of mesoconvective organization in section 4, multiscale models give insight into the mechanisms responsible for large-scale convective organization. Moncrieff (2004) showed that mesoconvective organization interlocked with Rossby-gyre dynamics explains the momentum transport and atmospheric superrotation properties that occurred in the Grabowski (2001) superparameterized global model. The reasons for superrotation was further quantified by Biello *et al.* (2006). The models of Yano et al. (1997) and Khouider and Majda (2007), characterized by a passive boundary layer, a dynamically active troposphere, and simple parameterizations of convection, radiation, boundary-layer and surface exchange. Both models generate large-scale convective coherence: an eastward-traveling convective envelope and westward-traveling synoptic-scale disturbances. The second-baroclinic modes in Khouider and Majda produce more realistic large-scale coherence than in Yano et al. , where the troposphere has a first-baroclinic vertical structure. Convectively-coupled moist gravity wave-trains and the cloud-envelope

propagate at realistic speeds. Growth rates at low zonal wave numbers indicate strong wave-wave interaction.

c) Parameterizing convective organization

The above examples of CRM simulations show convective organization to be important in the large-scale atmospheric circulation. For computational reasons the explicit representation of convection in length climate model integrations will be impractical for the foreseeable future. It follows that convective organization should be represented in parameterizations. New approaches are required, not tinkering with existing methods for the following reasons: i) the existence of mesocale convective organization is contrary to the assumption of scale-separation between cumulus and the grid-scale; ii) cumulus convection and organized convection are morphologically distinct (Fig. 7).

The explicit approach is superparameterization is a new approach. Another is the hybrid approach in which cumulus parameterization and explicit circulations exist concurrently. The hybrid approach is particularly suitable for models with a ~10 km grid spacing (next-generation NWP models and future climate models) where the mesoscale organization is reasonably realistic. Moncrieff and Klinker (1997) showed that explicit superclusters may occur in a global prediction model at a 80-km grid-spacing, and dominate the convective parameterization. The hybrid representation of Moncrieff and Liu (2006) approximates stratiform heating, mesoscale downdrafts and momentum transport by convective organization. Kruell et al (2007) produced a mass-flux based hybrid parameterization.

While traditional parameterizations are mainly deterministic, they have stochastic connotations because deep convection is a "fast" process with limited predictability compared with the "slow" evolution of the mean state. Shutts and Palmer (2007) used CRM simulations to evaluate the extent to which deterministic convective parameterizations fail to

capture statistical fluctuations, and provided probability distribution functions that may be used in stochastic parameterizations for global models.

10. Future developments

Much more work remains to be done on comparing simulated cloud systems over various types of land and vegetation environments. Recently completed field programs (TOGA-COARE, LBA, KWAJEX, TRMM SCSMEX, TC4, CAMEX, TCSP, TC4, AMMA, ARM, and TWP-ICE) should provide a good opportunity to orchestrate combined observational and numerical studies of convective systems. These large-scale field campaigns can provide some of the desperately needed observations for key locations. These observations can guide and correct existing microphysical schemes used in the CRMs.

In addition, many recent and future earth-observing missions (including many NASA satellite programs) can provide measurements of clouds, radiation, precipitation, aerosols, land characteristics and other data at very fine spatial and temporal scales globally. Since the CRM can explicitly simulate cloud processes at the natural space and time scales of cloud-dynamical processes, cloud statistics, including radiances and radar reflectivities/attenuation, can be directly extracted from the CRM-based physics and compared against measurements. It is also encouraged to estimate satellite-consistent signals using radiative transfer (i.e., satellite simulators) using the consistent model assumptions of microphysics (Chaboureau *et al.* 2002; Chevallier and Bauer 2003), since the satellite direct measurements hold much less uncertainties in comparison with the retrieved physical parameters.

a) Improving CRMs

Current CRMs reasonably simulate the evolution, structure, and life cycles of cloud systems. They can also explicitly calculate the interaction between clouds, longwave and solar radiation that are difficult, if not impossible, to measure observationally. However, Cotton (2003) has discussed some of the limitations (i.e., prediction of ice particle concentrations

and their effect on ice processes, initial broadening of cloud droplet spectra in warm clouds, details of hydrometeor spectra evolution, quantitative simulations of entrainment rates) of current CRMs. These limitations (or deficiencies) must be resolved in the coming years. In addition, cloud microphysical processes, heat fluxes from the warm ocean, land and radiative transfer processes should interact with each other explicitly. How these processes interact under different environmental conditions should be a main focus of modeling studies in the future. Also, a major area in need of development involves scale interactions and how cloud processes must be included in simulations of mesoscale to global-scale circulation models.

b) CRM research and applications

Many current CRMs need large-scale advective forcing in temperature and water vapor, either from intensive sounding networks that are deployed during major field experiments or from large-scale model analyses, to be imposed as an external forcing (termed "*a semi-prognostic approach*", see Soong and Tao 1980). The advantage of this approach is that model results in terms of rainfall, temperature and water vapor budget are usually in good agreement with observations (see Tao 2003 for a brief review and Randall *et al.* 2003a). However, CRM simulations with observed forcing only allow one-way interaction and cannot address the effects of cloud and radiation feedbacks on GCMs.

Grabowski and Smolarkiewicz (1999); Khairoutdinov and Randall (2001); and Randall *et al.* (2003b) proposed a multi-scale modeling framework (MMF, termed "*super parameterization*"), which replaces the conventional cloud parameterizations with a CRM in each grid column of a GCM. The use of a GCM enables global coverage, while the CRM allows for better and more sophisticated physical parameterizations (i.e., CRM-based physics). Therefore, the MMF can explicitly simulate deep convection, cloudiness and cloud overlap, cloud-radiation interaction, surface fluxes, and surface hydrology at the resolution of a CRM. It also has two-way interactions between the CRMs and their parent GCM. **Figure XX** shows the geographical distribution of the local solar time (LST) of the non-drizzle precipitation frequency maximum in winter and summer of 1998 as simulated by a GCM,

and two different MMFs (Goddard and CSU MMF). Both MMFs are superior to the GCM in reproducing the correct timing of the late afternoon and early evening precipitation maximum over land and the early morning precipitation maximum over the oceans. The GCM, in contrast, produces a dominant morning maximum rain frequency over major continents.

The MMF could also be a natural extension of current cloud resolving modeling activities. MMFs can also bridge the gap between traditional CRM simulations and current and future non-hydrostatic global cloud-resolution models. For example, a global non-hydrostatic grid model with icosahedral structure is being developed in Japan (Satoh *et al.* 2005). This model is intended for high-resolution climate simulations with cloud-resolving physical processes (i.e., cloud microphysics, radiation, and boundary layer processes[15]). It has been performed on an aqua planet setup with grid intervals of 7 and 3.5 km. The model simulates reasonable features in the Tropics, like the hierarchical structure of clouds, and intra-seasonal oscillations (Tomita *et al.* 2005, Miura *et al.* 2005; Nasuno *et al.* 2007). It is expected that a close collaboration between CRMs, MMFs and non-hydrostatic high-resolution global cloud resolving models can enhance our ability to simulate realistic weather and climate in near future.

While CRMs explicitly simulate cloud dynamics and microphysics evolutions interactively, many uncertainties in cloud microphysics processes exist due to lack of practical evaluation frameworks that integrate CRM simulations and routine, extensive observations. In addition, cloud microphysical processes, fluxes from the warm ocean, land and radiative transfer processes should interact with each other explicitly. How these processes interact under different environmental conditions should be a main focus of modeling studies in the future. Also, a major area of needed development involves scale interactions and how cloud processes must be included in simulations of mesoscale to global-scale circulation models.

b) Model validation

---

15 MMFs can be used to identify the optimal grid size and physical processes (i.e., microphysics, cloud-radiation interactions) needed for future non-hydrostatic global CRMs.

The large computational domains (up to global) and the high-resolution of modern CRMs pose new problems form model validation against observations. Both field-campaign and satellite databases are required, but these datasets are typically not in forms that are useful comparing against models. In order to address this formidable challenge, WCRP and WWRP/THORPEX are organizing a year of coordinated observing, modeling and forecasting with a focus on organized tropical convection and its prediction (*Year of Tropical Convection, YOTC*). The intent is to exploit the vast amounts of existing and emerging observations, the expanding computational resources and the development of new, high-resolution modeling frameworks. This focused activity will benefit from the coordination of a wide range of ongoing and planned international programmatic activities, and collaboration among the operational prediction, research laboratory and academic communities. The timing, focus-year approach and integrated framework of YOTC will leverage the most benefit from recent major investments in Earth science infrastructure. Another motivation is to motivate a new generation of scientists to tackle key challenges of relevance to Earth-system science. The first YOTC activity is the construction of a comprehensive global database of satellite data and high-resolution model analysis and forecasts. In some respects, YOTC is the modern equivalent of the tropical components of the First GARP Global Experiment (FGGE). The global nature of the database and accompanying research will advance basic knowledge, diagnosis, modeling, parameterization and prediction of multi-scale convection and two-way interaction between the tropics and extra-tropics relevant to both weather and climate.

- Derive physically based parameterizations for large-scale models (i.e., general circulation models and climate models);
- Test single-column representations of physical processes (i.e., the processes that trigger convection, cloudiness and convective momentum transport);
- Complement large-scale field experiments that would otherwise be sub-critical in terms of cloud-scale measurements;
- Add value to data sets in situations where standard soundings are the only measurement available;
- Utilize the multi-satellite data simulators to identify key interactive processes between cloud, precipitation and aerosol;

- Improve the physical basis of surface (land and ocean)-atmosphere interaction in coupled general circulation models and climate models;
- Help in the design of space-based and earth-based remote sensing and in the interpretation of the data sets; and
- Understand the cloud and mesoscale vortex formation that may be important for initial tropical cyclone (hurricane) development.

Advances in computing power allow numerical weather prediction (NWP) models to be run at progressively finer scales of resolution, using increasingly more sophisticated physical parameterizations. The representation of cloud microphysical processes is a key component of these models, over the past decade both research and operational NWP models [i.e., the Fifth-generation National Center for Atmospheric Research (NCAR)/Penn State University Mesoscale Model (MM5), the National Centers for Environmental Prediction (NCEP) Eta, and the Weather Research and Forecasting Model (WRF)] have started using more complex microphysical schemes that were originally developed for high-resolution CRMs. A report to the United States Weather Research Program (USWRP) Science Steering Committee specifically calls for the replacement of implicit cumulus parameterization schemes with explicit bulk microphysical schemes in NWP as part of a community effort to improve quantitative precipitation forecasts (QPF, Fritsch and Carbone 2002).

11. Conclusions

Cloud-system resolving models originated as cloud-process models, have advanced greatly in the past four decades, and will be the basis of global weather prediction models within a decade or so, and eventually climate model. Global CRMs have already been run on an experimental basis.

References:

Benjamin, T.B., 1968: Gravity currents and related phenomena. *J. Fluid Mech.*, **31**, 209-248.

Biello, J., A. J. Majda, and M.W. Moncrieff, 2007: Meridional momentum flux and superrotation in the multiscale IPESD MJO model. *J. Atmos. Sci.*, **64**, 1636–1651.

Carbone, R.E., 1982: A severe winter squall line: Stormwide hydrodynamic structure. *J. Atmos. Sci.*, **39**, 258-279.

Chen, Y., A. D. del Genio, and J. Chen, 2007: The tropical atmospheric El Nino signal in satellite precipitation data and a global climate model. *J. of Climate*, **20**, 3580-3601.

Cotton, W.R., and R.A. Anthes, 1989: Storm and Cloud Dynamics, 881 pp, Academic, San Diego, Calif.

Haertel, P. T., and G.N. Kiladis, 2004: Dynamics of 2-Day Equatorial Waves. *J. Atmos. Sci.*, **61**, 2707-2721.

Houze, R. A., Jr., C.-C. Cheng, C. A. Leary, and J. F. Gamache, 1993: Diagnosis of cloud mass and heat fluxes from radar and synoptic data. *J. Atmos. Sci.*, **37**, 754-773.

Houze, R. A., Jr., 2004: Mesoscale convective systems. *Rev. Geophys.*, **42**, RG4003, doi:101029/2004RG000150.

Houze, R. A., Jr., C.-C. Cheng, C. A. Leary, and J. F. Gamache, 1980: Diagnosis of cloud mass and heat fluxes from radar and synoptic data. *J. Atmos. Sci.*, **37**, 754-773.

Grabowski, W.W., 2001: Coupling cloud processes with the large-scale dynamics using the Cloud-resolving Convection parameterization (CRCP). *J. Atos. Sci.*, **58** , 978-997.

Grabowski, W.W., and M.W. Moncrieff 2001: Large-scale organization of tropical convection in two-dimensional explicit numerical simulations. *Quart. J. Roy. Meterol. Soc.*, **127**, 445-468.

Grabowski, W. W., X. Wu, M. W. Moncrieff, and W. D. Hall, 1998: Cloud-resolving modeling of cloud systems during Phase III of GATE. Part II: Effects of resolution and the third spatial dimension. *J. Atmos. Sci.*, **55**, 3264-3282.

Hou, A. Y., and S. Q. Zhang, 2007: Assimilation of precipitation information using column model physics as a weak constraint. *J. Atmos. Sci.*, **64**, 3865-3878.

Iguchi, T., R. Oki, E.A. Smith and Y. Furuhama, 2002: Global Precipitation Measurement program and the development of dual-frequency precipitation radar. *J. Commun. Res. Lab. (Japan),* **49**, 37-45.

Jones, J. and R. Meneghini, 1997: Synthetic data for testing TRMM radar algorithms. Proc. 28th Conf. Radar Meteorology, 196-197, AMS, Austin, TX.

Kiladis, G. N, K.H. Straub, and P. T. Haertel, 2005: Zonal and vertical structure of the Madden-Julian Oscillation *J. Atmos. Sci.,* **62**, 2790-2809.

Khairoutdinov, M., D. A. Randall, and C.DeMott, 2005: Simulations of the atmospheric general circulation using a cloud-resolving model as a superparameterization of physical processes. *J. Atmos. Sci.,* **62**, 2136-2154.

Khouider, B., and A. J. Majda, 2007: A simple multicloud parameterization for convectively coupled tropical waves. Part II: Nonlinear simulations. *J. Atmos. Sci.,* **64**, 381–400.

Kozu et al., 2001: Development of precipitation radar onboard the Tropical Rainfall Measuring Mission (TRMM) Satellite. *IEEE Geosc. Remote Sensing*, **39**, 102-116.

Kuell, V., A. Gassmann, A. Bott, 2007: Towards a new hybrid cumulus parametrization scheme for use in non-hydrostatic weather prediction models. *Quart. J. Roy. Meteor. Soc.,* **133**, 479-490.

Kumagai, H., R. Meneghini, and T. Kozu, "Preliminary results from multiparameter airborne rain radar measurement in the western Pacific," *J. Appl. Meteor.*, vol. 32, pp. 701-711, 1994.

Lafore, J.P., J-L. Redelsperger, and G. Jaubert, 1988: Comparison between a Three-Dimensional Simulation and Doppler Radar Data of a Tropical Squall Line: Transports of Mass, Momentum, Heat, and Moisture. *J. Atmos. Sci.*, 43, 3483-3500.

Laing, A.G., and J.M. Fritsch, 1997: The global population of mesoscale convective complexes. *Quart. J. Roy. Meteor. Soc.,* **123**, 389-405.

Lane, T.P., and M. J. Reeder, 2001: Convectively generated gravity waves and their effect on the cloud environment. *J. Atmos. Sci.,* **58**, 2427–2440.

LeMone, M.A., and M.W. Moncrieff, 1993: Momentum and mass transport by convective bands: Comparisons of highly idealized dynamical models to observations. *J. Atmos. Sci.*, **51**, 281-305.

Lin, J.-L., G. N. Kiladis, B. E. Mapes, K. M. Weickmann, K. R. Sperber, W. Lin, M.C. Wheeler, S. D. Schubert, A Del Genio, L. J. Donner, S. Emori, J-F. Gueremy, F. Hourdin, P.J. Rasch, E. Roeckner, and J. F. Scinocca, 2006: Tropical intraseasonal variability in 14 IPCC AR4 climate models. Part I: Convective signals. *J. Climate*
19, 2665–2690.

Liu, C. and M.W. Moncrieff, 2004: Effects of convectively generated gravity waves and rotation on the organization of convection. *J. Atmos. Sci.*, **61**, 2218-2227.

Ludlam, F.H., 1980: *Clouds and Storms: The behavior and effect of water in the Atmosphere*, 405 pp., Pa. State Univ. Press, University Park, Pa.

Madden, R., and P. Julian, 1972: Description of global-scale circulation cells n the Tropics with a 40-50 day period. *J. Atmos. Sci.,* **29**, 1109-1123.

Mapes, B.E., 1993: Gregarious tropical convection. *J. Atmos. Sci.,* 50, 2026–2037.

Mardiana, R., T. Iguchi, N. Takahashi, and H. Hanado, 2003: Dual-frequency rain profiling method without the use of surface reference technique. *Proc. IGARSS'03.*

Meneghini, R., T. Kozu, H. Kumagai, and W. C. Boncyk, 1992: A study of rain estimation methods from space using dual-wavelength radar measurements at near-nadir incidence over ocean, *J. Atmos. Oceanic Technol.*, **9**, 364-382.

Meneghini, R., J.A. Jones, T. Iguchi, K. Okamoto, and J. Kwiatkowski, 2004: A hybrid surface reference technique and its application to the TRMM Precipitation Radar. *J. Atmos. Oceanic Technol.*, **21**, 1645-1658.

Meneghini, R., Status of synthetic data for testing of TRMM Radar Algorithms, Proc. Second Joint Radar Team Meeting, Aug. 16-18, 1996, NASA/GSFC.

Meneghini, R. and L. Liao, "Effective dielectric constants of mixed-phase hydrometers," *J. Atmos. Oceanic Technol.,* **17**, 628-640, 2000.

Moncrieff, M.W., 1981: A Theory of Organized Steady Convection and its Transport Properties. *Quart. J. Roy. Meteor. Soc.*, **107**, 29-50.

Moncrieff, M.W., 1992: Organized convective systems: archetypal dynamical models, mass and momentum flux theory, and parameterization. *Quart. J. Roy. Meterol. Soc.,* **118**, 819-950.

Moncrieff, M. W., 1997: Momentum transport by organized convection. *NATO Advanced Study Series: C. The Physics and Parameterization of Moist Atmospheric Convection* (R. Smith, Ed.), Klumer Academic Publishers, Netherlands, 231-253.

Moncrieff, M.W., 2004: Analytic representation of the large-scale organization of tropical convection. *J. Atmos. Sci.,* **61**, 1521-1538.

Moncrieff, M.W., and J.S.A. Green, 1972: The propagation and transfer properties of steady convective overturning in shear. *Quart. J. Roy. Meteor. Soc.*, **97**, 336-352.

Moncrieff, M.W., and M. J. Miller, 1976: The dynamics and simulation of tropical cumulonimbus and squall-lines. *Quart. J. Roy. Meteor. Soc.*, **102**, 373-394.

Moncrieff, and E. Klinker, 1997: Mesoscale cloud systems in the Tropical Western Pacific as a process in general circulation models. *Quart. J. Roy. Meteorol. Soc.*, **123**, 805-827.

Moncrieff, M.W., and C. Liu, 2006: Representing convective organization in prediction models by a hybrid strategy. *J. Atmos, Sci.,* **63**, 3404-3420.

Morita, J., Y. N. Takayabu, S. Shige, and Y. Kodama, 2006: Analysis of rainfall characteristics of the Madden-Julian oscillation using TRMM satellite data. *Dyn. Atmos. Oceans*, **42**, 107-126.

Moncrieff, M.W., M. Shapiro, J. Slingo, and F. Molteni, 2007: Collaborative research at the intersection of weather and climate. *WMO Bulletin*, **56**, 204-211.

Nakazawa, T., 1988: Tropical superclusters within intraseasonal variations over the western Pacific. *J. Meteor. Soc. Japan*, **66**, 823-839.

Nesbitt, S. W., R. Cifelli, and S. A. Rutledge: 2006: Storm morphology and rainfall characteristics of TRMM precipitation features. *Mon. Wea. Rev.*, **134**, 2702-2721.

Nicholls, M.E., R.A. Pielke, and W. R. Cotton, 1991: Thermally forced gravity waves in an atmosphere at rest. *J. Atmos. Sci.,* **48**, 1869–1884.

Iguchi, T., T. Kozu, R. Meneghini, J. Awaka, and K. Okamoto, 2000: Rain profiling algorithm for the TRMM Precipitation Radar. *J. Appl. Meteor.*, **39**, 2038-2052.

Olson, W.S., P. Bauer, N. F. Viltard, D. E. Johnson, W.-K. Tao, R. Meneghini, and L. Liao, 2001: A melting-layer model for passive/active microwave remote sensing applications. Part I: Model formulation and comparison with observations, *J. Appl. Meteor.*, **40**, 1145-1163.

Rajendran, R., T.N. Krishnamurti, V. Misra, and W.-K. Tao, 2004: An empirical cumulus parameterization scheme based on TRMM latent heating profiles. *J. Meteor. Soc. Japan*, **82**, 989-1006.

Redelsperger, J.-L. and J-P. Lafore, 1988: A Three-Dimensional Simulation of a Tropical Squall Line: Convective Organization and Thermodynamic Vertical Transport. *J. Atmos. Sci.*, 45, 1334–1356.

Shutts, G.J., and T. N. Palmer, 2007: Convective forcing fluctuations in a cloud-resolving model: Relevance to the stochastic parameterization problem. *J. Climate*, 20, 187–202.

Smith, R.K., 1997: *The Physics and Parameterization of Moist Atmospheric Convection,* 498pp, NATO ASI Series, 505, Kluwer Academic Publishers, Dordecht/Boston/London.

Straub, K.H., and G.N. Kiladis, 2002: Observations of a convectively coupled Kelvin wave in the Eastern Pacific ITCZ. *J. Atmos. Sci.*, 59, 30-53.

Thorpe, A. J., M. J. Miller, and Moncrieff, M.W., 1980: Dynamical Models of Two-dimensional Updraughts and Downdraughts. *Quarterly Journal of the Royal Meteorological Society*, **106**, 463-484.

Thorpe, A. J., M. J. Miller, and Moncrieff, M.W., 1982: Two-dimensional Convection in Non-constant Shear: A Model of Mid-latitude Squall Lines. *Quart. J. Roy. Meteor. Soc.*, 108, 739-762.

Tulich, S.N., D. A. Randall, and B. E. Mapes, 2007: Vertical-mode and cloud decomposition of large-scale convectively coupled gravity waves in a two-dimensional cloud-resolving model. *J. Atmos. Sci.*, 64, 1210–1229.

Wu, X., W.W. Grabowski, and M.W. Moncrieff, 1998: Long-term behavior of cloud systems in TOGA COARE and their interactions with radiative and surface processes. Part I: Two-dimensional Modeling Study. *J. Atmos. Sci.*, **55**, 2693-2714.

Yano, J. I., J. C. McWilliams, M. W. Moncrieff, and K. A. Emanuel, 1995: Hierarchical tropical cloud systems in an analog shallow-water model. *J. Atmos. Sci.*, 52, 1724-1742.

Zipser, E. J., 1977: Mesoscale and convective-scale downdrafts as distinct components of squall-line structure. *Mon. Wea. Rev.*, 105, 1568-1589.

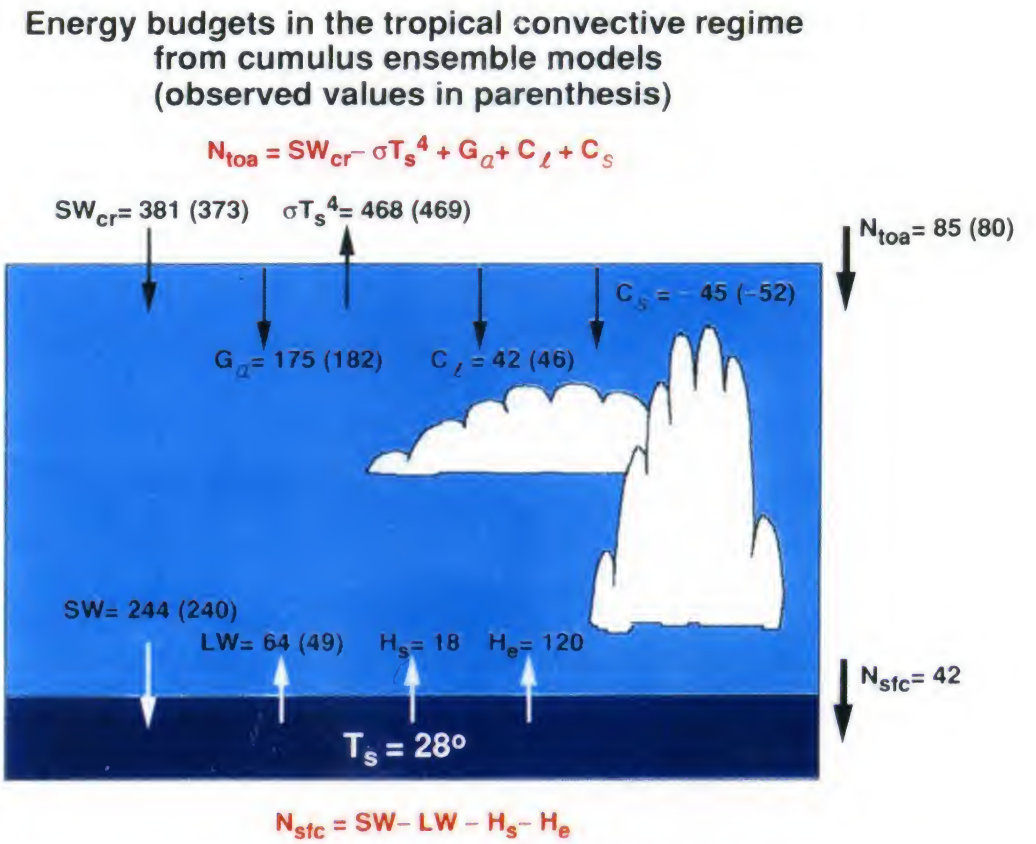

Figure 1: Energy fluxes at the top of the atmosphere and at the ocean-atmosphere interface as computed by the Goddard Cumulus Ensemble (GCE) model. Also included in parenthesis are top-of-the-atmosphere fluxes estimated from ERBE and surface flux estimates from Radiation model for April 1985. The observed values (in parenthesis) are averaged over the region from 100°E to 180°E, 20°N to 20°S. Subscripts "toa" denotes top of atmosphere, "CR" for clear sky condition, and "sfc" for surface. SWcr is the net absorbed solar radiation averaged over clear sky region. Ts^4 is the longwave radiation emitted by the ocean surface. SW and LW stand for short-wave and long-wave radiative heating/cooling, respectively. Hs and He stands for surface sensitive and latent heating fluxes, respectively. Ga is the atmospheric greenhouse effect. Cs and Cl is the longwave and shortwave cloud forcing respectively. Units are in Wm^{-2}. Ts is ocean surface temperature. Reasonable agreement between modeled and satellite observed budget is found. [Adapted from Lau et al. (1994).]

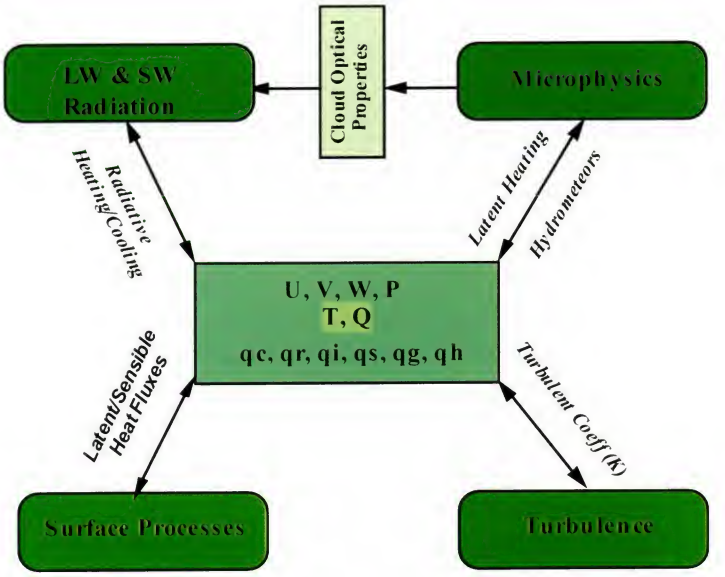

Figure 2: Schema showing the characteristics of cloud-resolving models. Arrows with sol lines indicate a two-way interaction between different physical processes. U,V,W and stand for horizontal winds, vertical wind and pressure, respectively. T and Q a atmospheric temperature and mixing ratio of the water vapor, respectively. Qc, qr,qi, qs,q and qh stand for the mixing ratio of cloud water, rain, cloud ice, snow, graupel and ha respectively (will be discussed in next section). LW and SW are atmospheric long and sho radiative cooling and heating, respectively. It is adapted from Tao (2007).

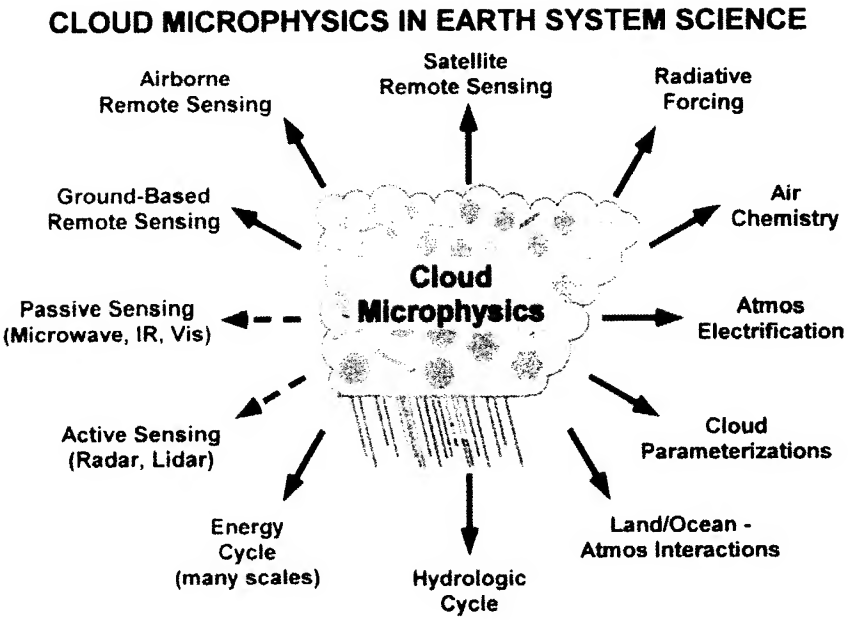

Figure 3: Schematic diagram of the role of cloud-microphysics in Earth-system science.

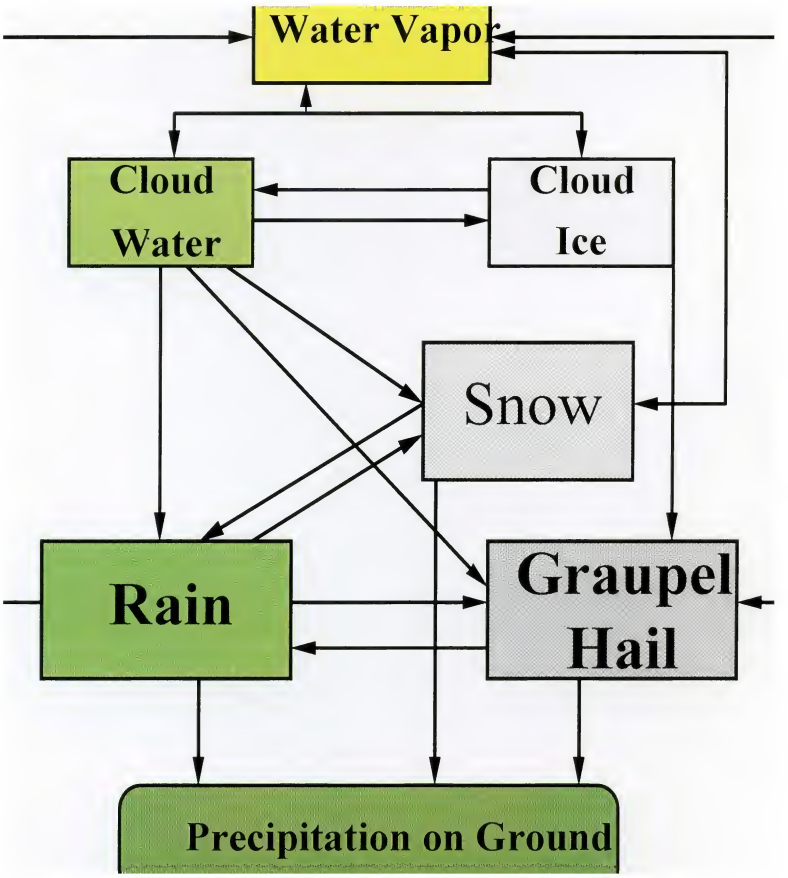
Water Vapor
Cloud Water
Cloud Ice
Snow
Rain
Graupel Hail
Precipitation on Ground

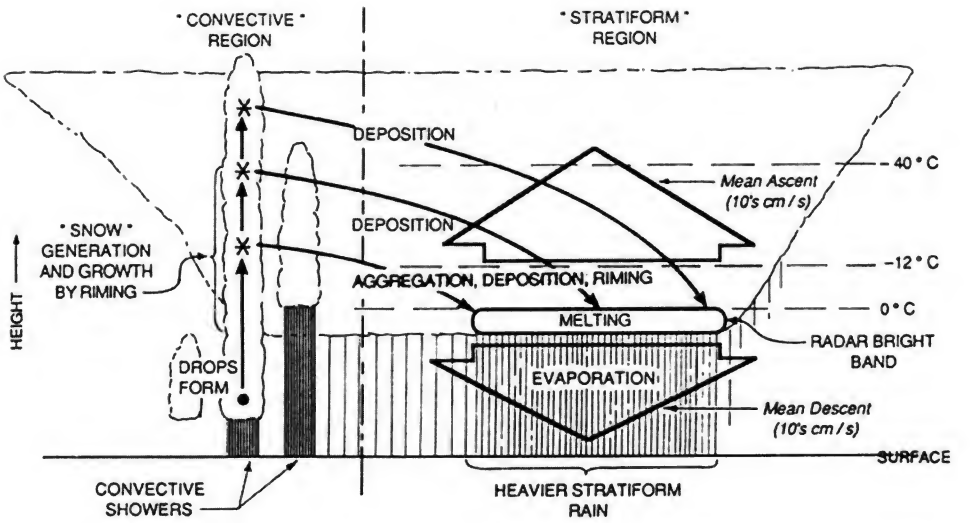

Figure 5: Schematic diagram of precipitation mechanisms of deep convective cells and the associated stratiform region for a mature tropical convective system Straight, solid arrows indicate convective updraft, wide, open arrows indicate mesoscale ascent and subsidence in the stratiform region where vapor deposition and evaporation occur. Solid arrows indicate particle trajectories. [Adapted from Houze (1989).]

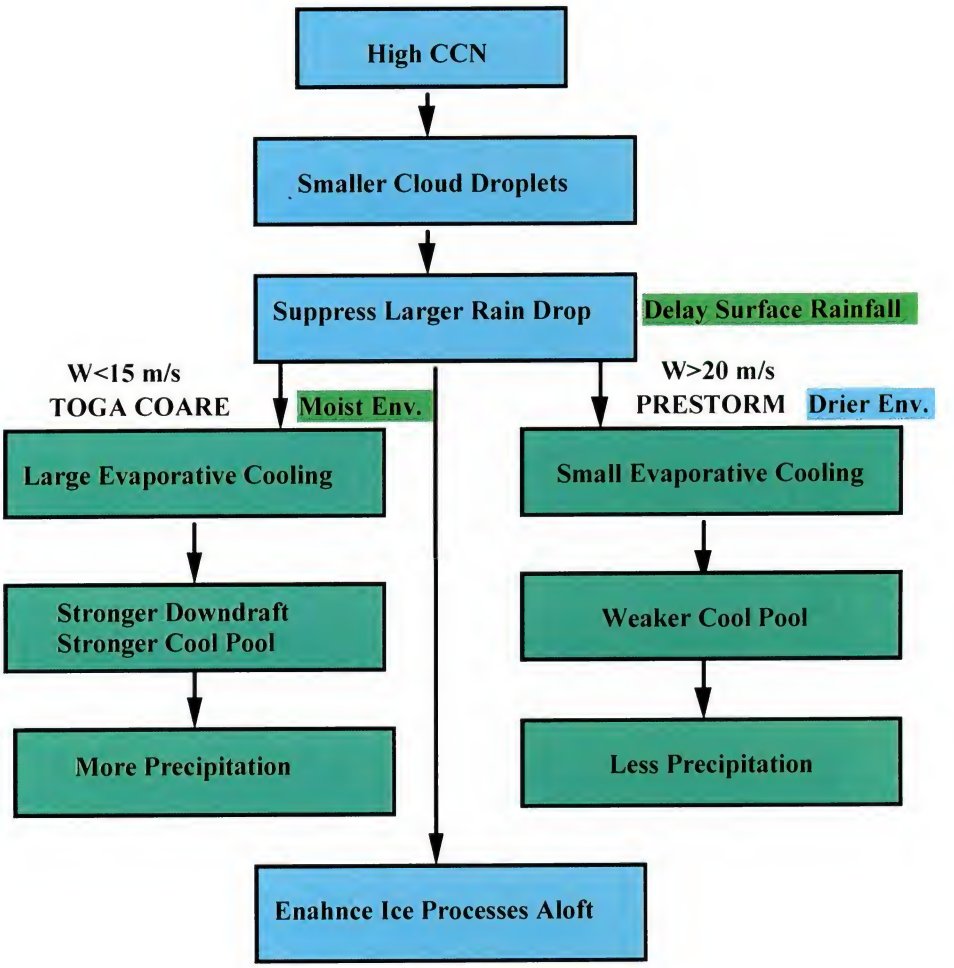

Figure 6: Schematic diagram showing the physical processes that lead to eithe enhancement (TOGA COARE case) or suppression (PRESTORM case) of precipitation in dirty environment. [Adapted from Tao et al. (2007).]

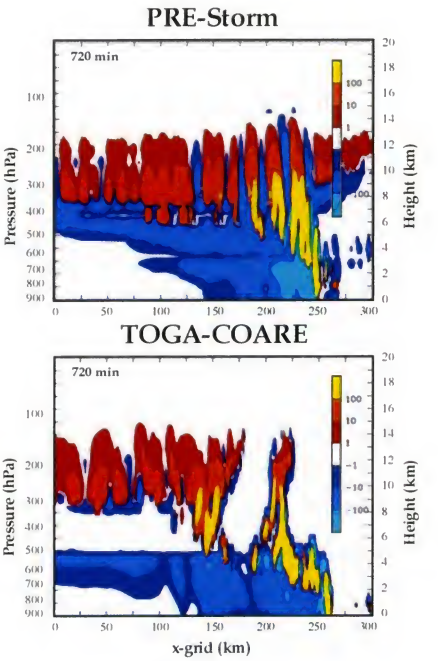

Figure 7: Height-length cross-sections of GCE-CRM-generated LH (°C day^{-1}) consisting o sum of heating by condensation, freezing, and deposition, and cooling by evaporatio melting, and sublimation -- associated with mid-latitude continental (PRE-STORM) squa line (upper panel) and tropical oceanic (TOGA-COARE) MCS (lower panel). [Simulatio are discussed in Tao et al. (1993a, 1995, 1996), Wang et al. (1996), and Lang et al. (2003) Adapted from Tao et al. (2006).

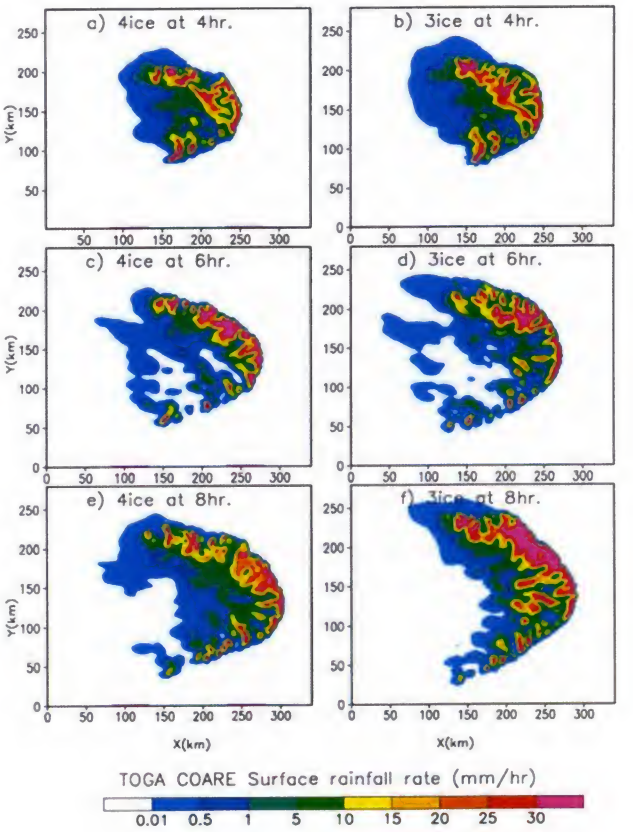

Figure 8: Surface rainfall rate (mm/h) simulated by a 3D CRM for a TOGA COARE squall system. ***(a)***, ***(b)*** *and* ***(c)*** *are for the 4ICE scheme at 4, 6 and 8 h, respectively, into the model simulation.* ***(d)***, ***(e)*** *and* ***(f)*** *are the same as (a), (b) and (c) except for the 3ICE scheme. The model domain consisted of 172 x 142 grid points in the horizontal x and y directions and the lateral boundaries were open. The horizontal grid resolution was 2 km. The vertical direction had 34 grid points up to 23.9 km stretched from 42.5 m at the lowest grid point to 1196 m at the top grid. Adapted from Tao et al. (2003).*

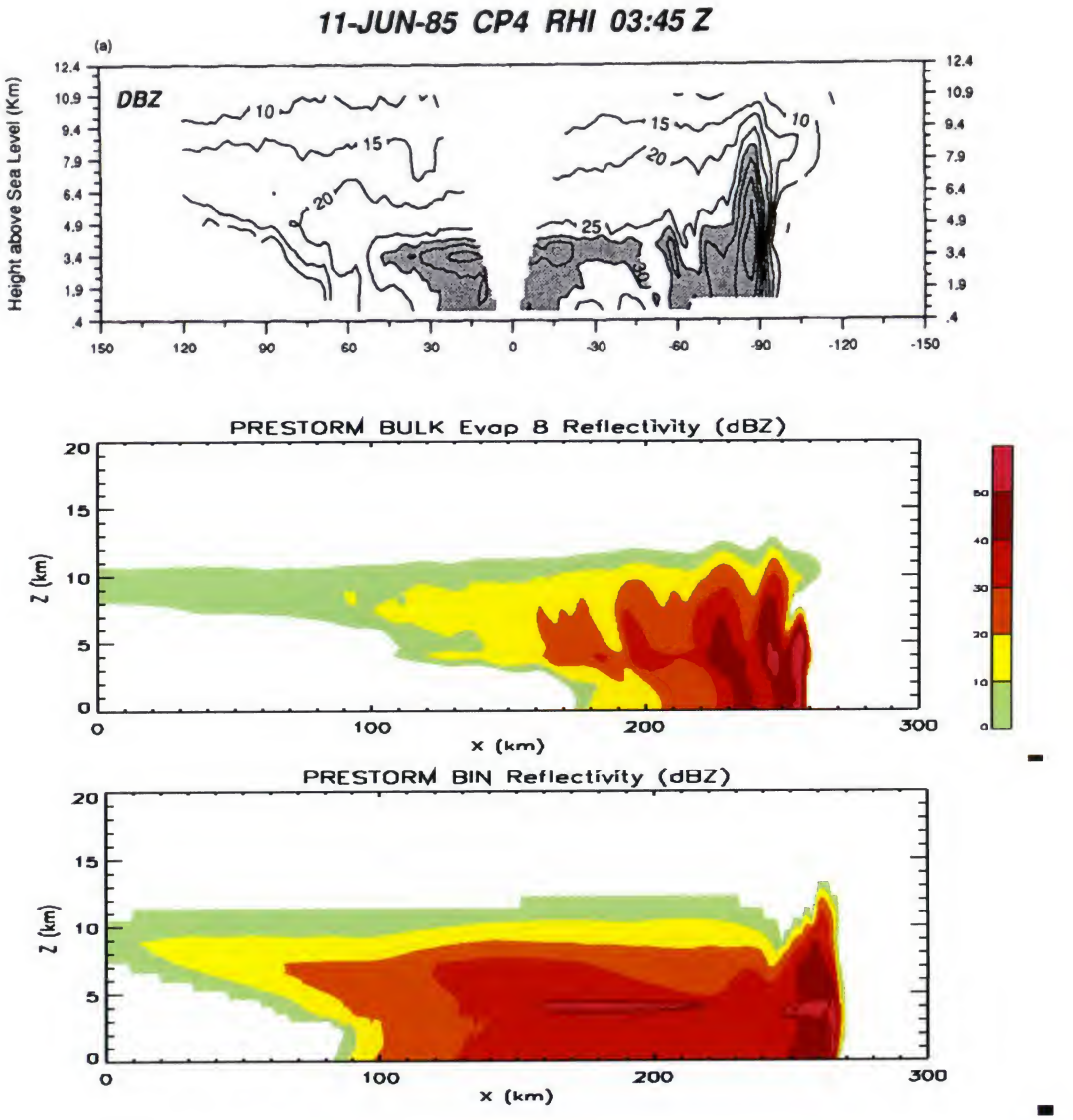

Figure 9: Top panel, the observed radar reflectivity at 3:45 UTC, 11 June 1985 during th mature stage of the PRE-STORM squall (Rutledge et al. 1988). Middle and lower panel CRM-simulated radar reflectivity with traditional one-moment 3ICE bulk scheme and th explicit spectral- bin microphysics scheme, respectively. Radar reflectivity in the bulk mod is calculated using fixed, exponential particle size distributions and densities, whereas th simulated particle size distributions are used in the bin model. The spatial scales an contour levels are matched in all 3 panels. [Adapted from Li et al. (2008a).]

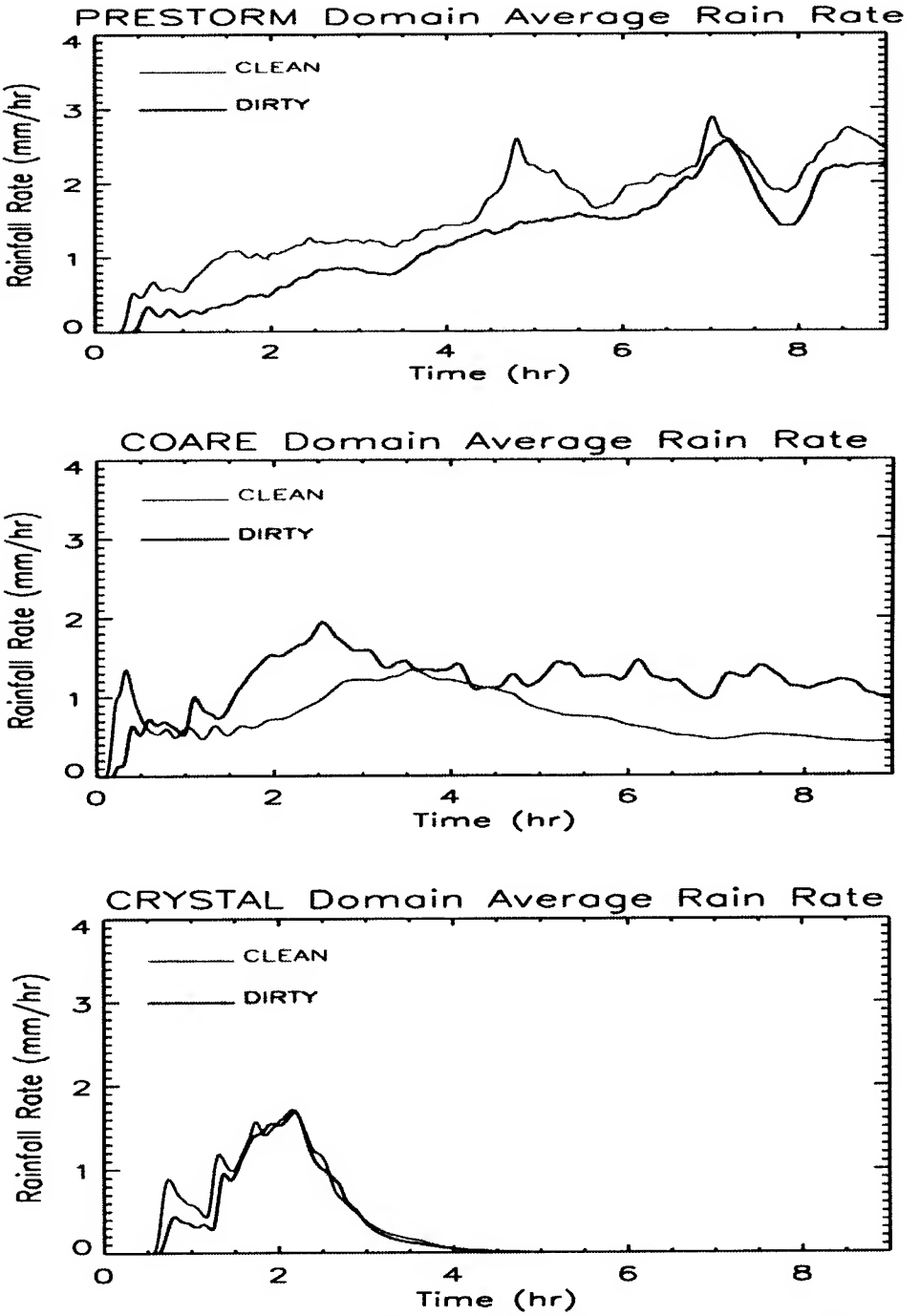

Figure 10: Time series of CRM-estimated domain mean surface rainfall rate (mm h^{-1}) for the (a) PRESTORM, (b) TOGA COARE, and (c) CRYSTAL case. The solid/dashed line represents clean/dirty conditions. [Adapted from Tao et al. (2007).]

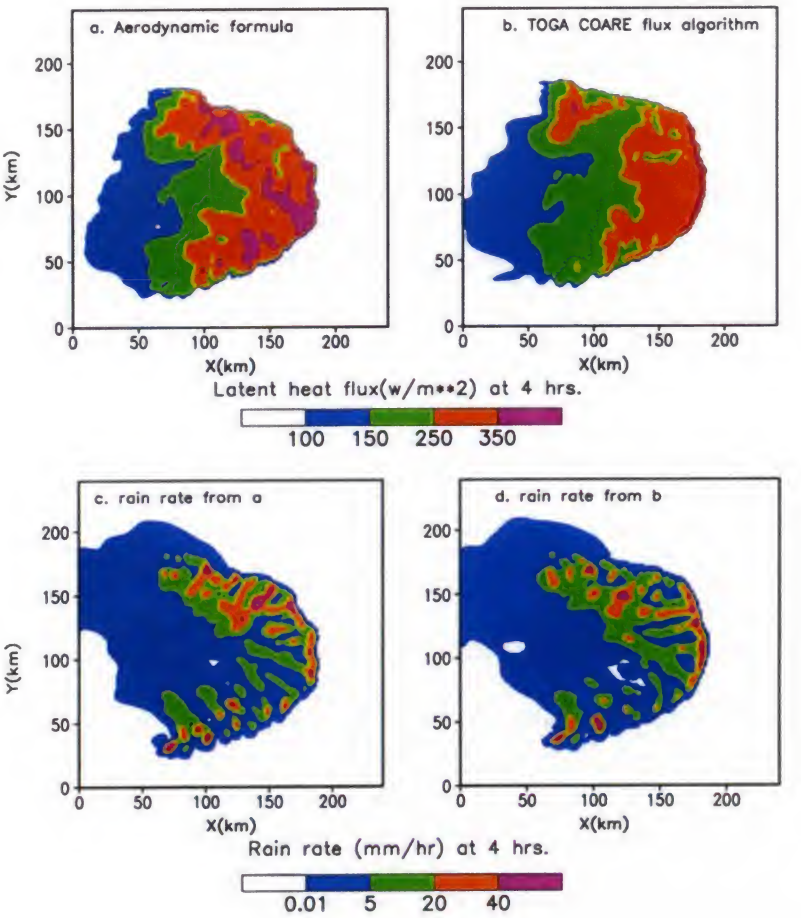

Figure 11: Surface latent heat flux at 6 hours into the simulation using (a) a simple bu aerodynamic method, and (b) the TOGA COARE flux algorithm. (c) and (d) are the same ((a) and (b) except showing the surface rain rate. [Adapted from Tao et al. (2003).]

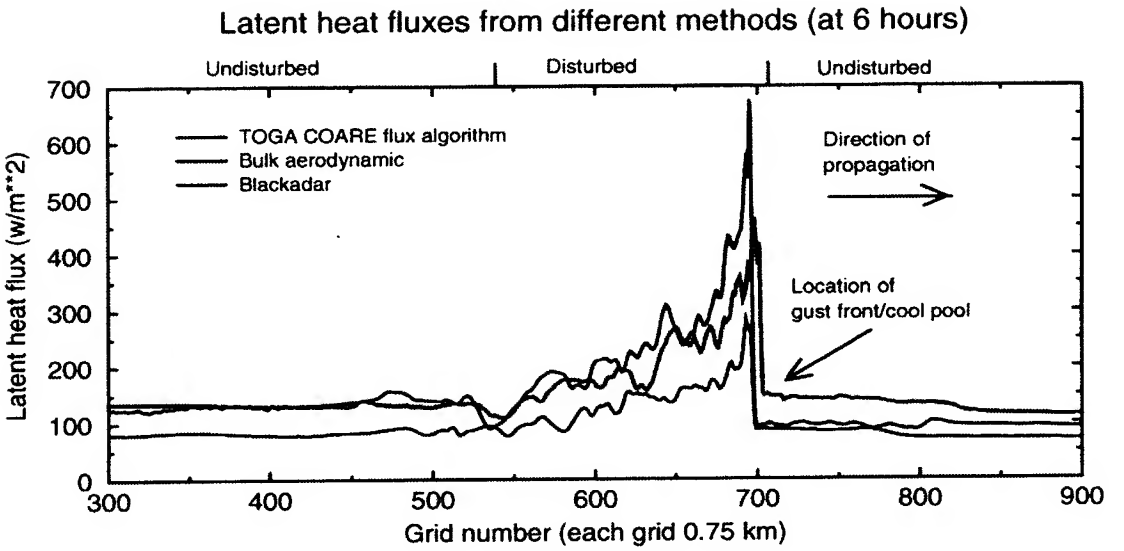

Figure 12: Latent heat fluxes simulated from different surface flux formulations at 6 hours [Adapted from Wang et al. (1996).]

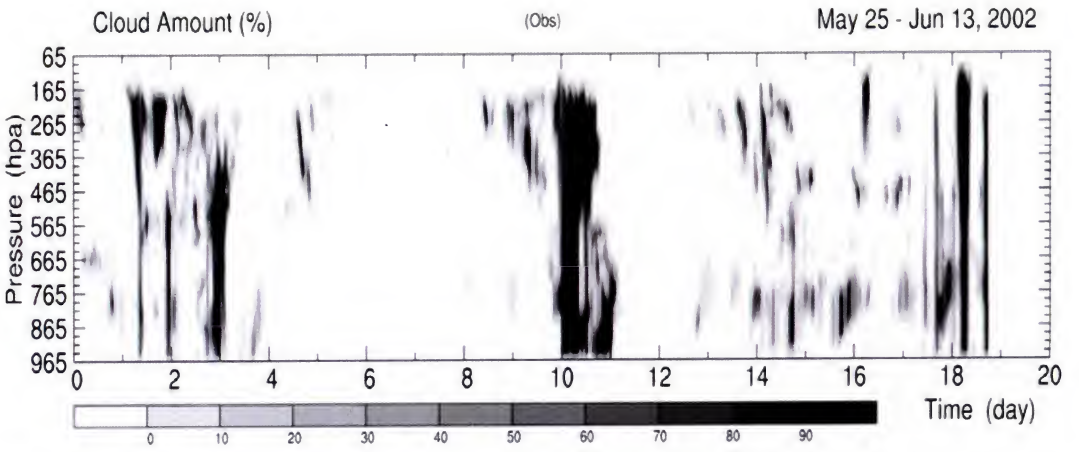

Figure 13: 20-day cloud simulation evaluated with ARM observations. Upper panel shows observed cloud amount. Middle and low panel modeled cloud amount with ARM and LIS surface fluxes as input, respectively. The results from numerical experiment with LIS capture observed cloud and precipitation processes especially for less-organized convective clouds. Adapted from Zeng et al. (2007).

TAO: Figure 13 has got messed up – please repair

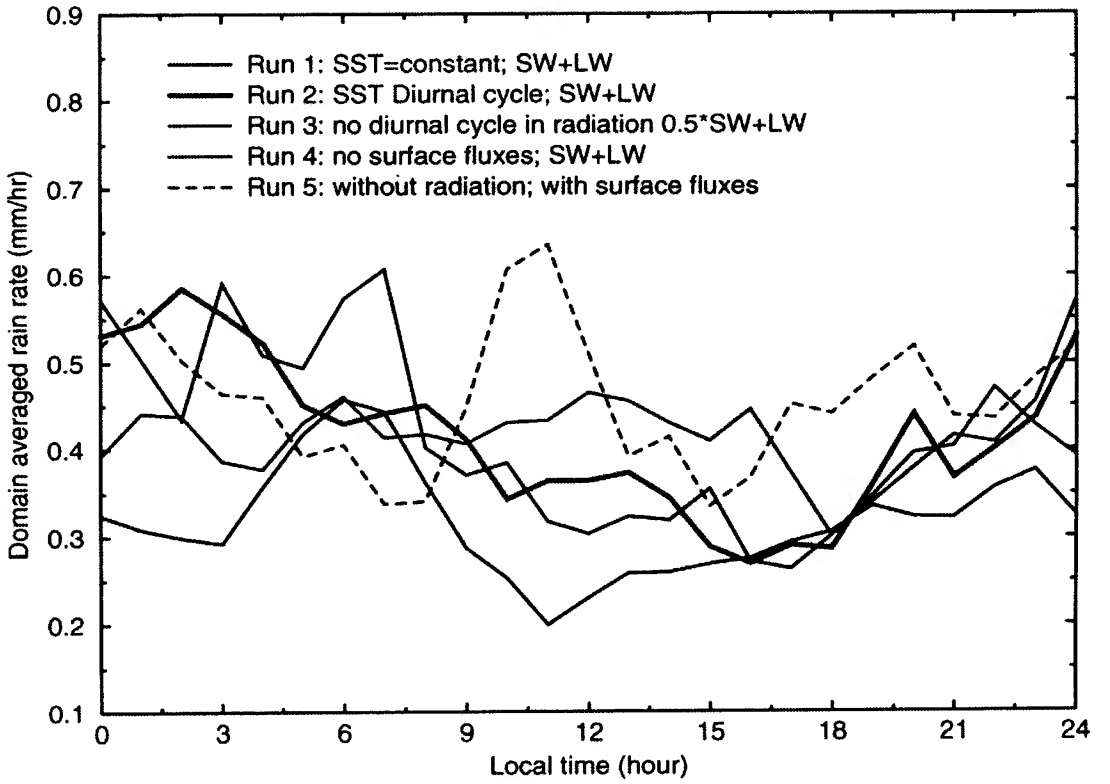

Figure 14: Diurnal composite of CRM domain averaged daily rain rate (mm h^{-1}). The (black) solid lines denote the run with constant sea surface temperature (SST - 29.2 °C) and explicit/diurnal cloud-radiation interaction. The red lines denote the run with diurnal SST variation (1 °C difference between the maximum and minimum) and explicit/diurnal cloud-radiation interaction. The green lines are for the run without SST diurnal variation and no diurnal variation in radiation. The blue lines denote the run without SST fluxes but with explicit/diurnal cloud-radiation interaction. The black dashed lines denotes the run without radiation but with surface fluxes. The initial thermodynamic conditions represented the disturbed periods during the TOGA COARE Intensive Observation Period (IOP) (upper-air soundings representing the disturbed periods were averaged). The large-scale vertical velocity for the same disturbed periods was also imposed into the CRM.

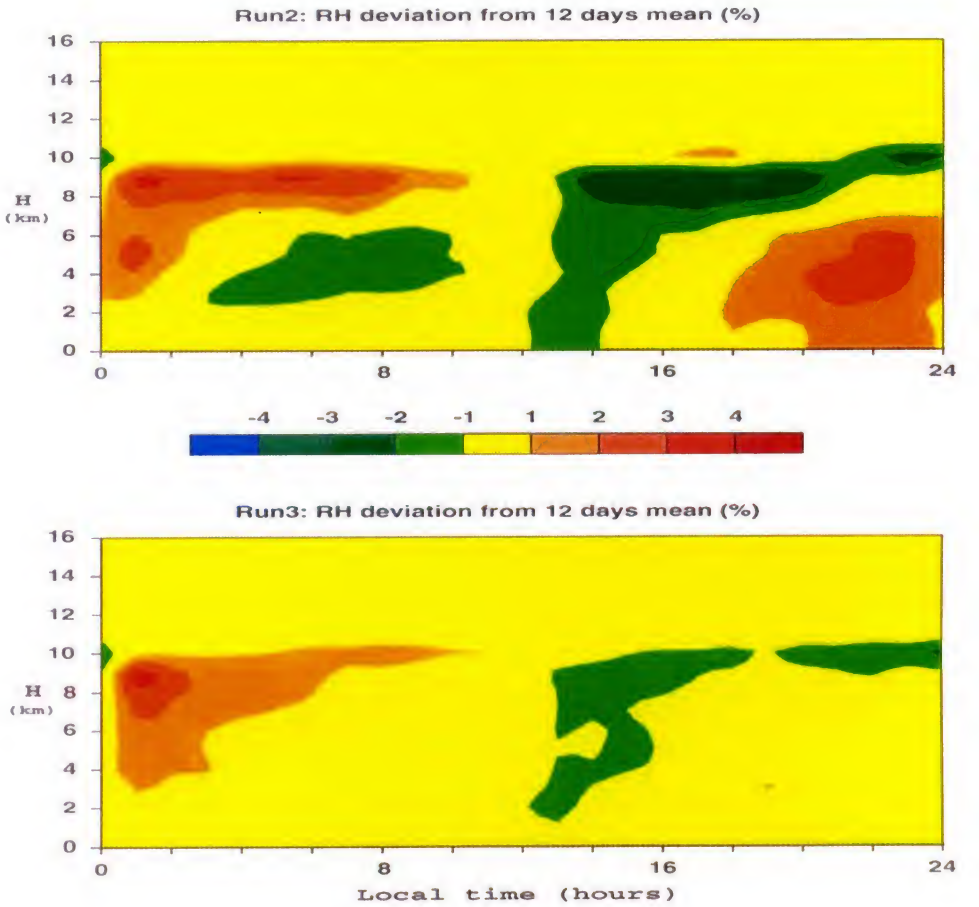

Figure 15: Diurnal composite of horizontal mean relative humidity (%) from the daily mean values obtained from a 12-day simulation. ***(a)*** *is for the run that allowed for the diurnal variation of radiative processes and* ***(b)*** *is for the run did not allow for the diurnal variation of radiative processes. Adapted from Tao et al. (2003).*

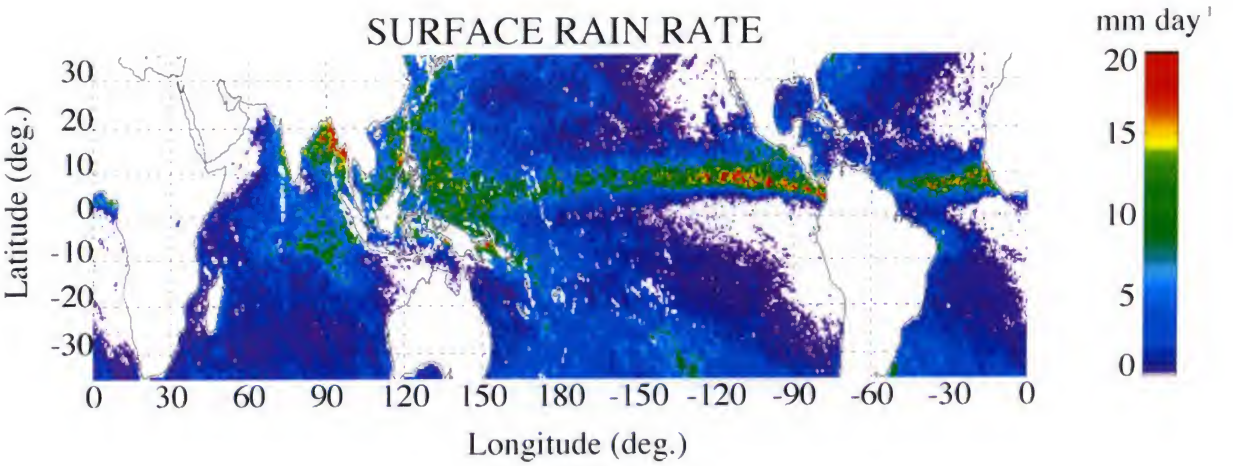

Figure 16: Three-month average retrieval of surface precipitation rate (Jun - Aug 2000) using GPROF Version 6, which utilized a cloud-resolving model database. The main features seen in this figure correspond to those seen in global climatology (e.g., Adler et al. 2003). Note the relative minima of convective proportion along the intertropical convergence zone. (ITCZ) and in the more rain regions of the western Pacific and Indian Ocean. These relative minima indicate a significant contribution to the total rainfall by organized mesoscale convective systems, as seen in Fig. 1 and described by Rickenbach and Rutledge (1998) in their analysis of radar observations from TOGA COARE field campaign. Adapted from Olson et al. (2006).

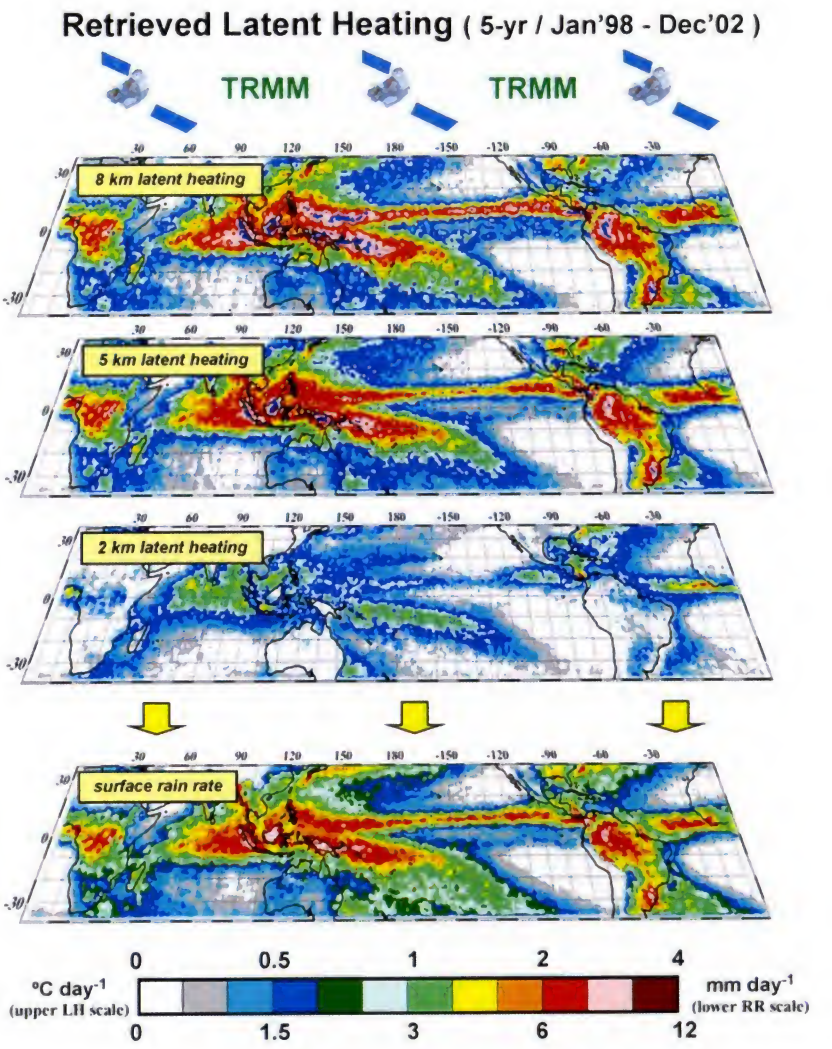

Figure 17: Upper two panels show the space-borne simulated 13.8 and 35 GHz radar reflectivity. Lower two panels show the ground-base simulated 13.8 and 35GHz radar reflectivity. Inputs of simulator from CRM simulation of a thunderstorm observed during the CRYSTAL-FACE.

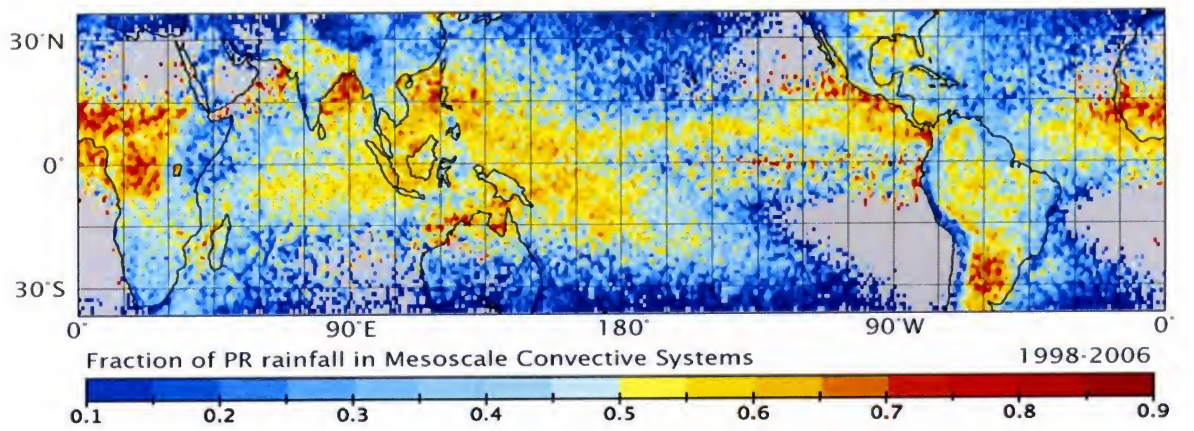

Figure 18: Fraction of estimated rainfall from precipitation features ≥ 100 km in maximum dimension as measured by the TRMM precipitation radar (PR) from January 1998 through December 2006 using the methodology of Nesbitt et al. (2006).

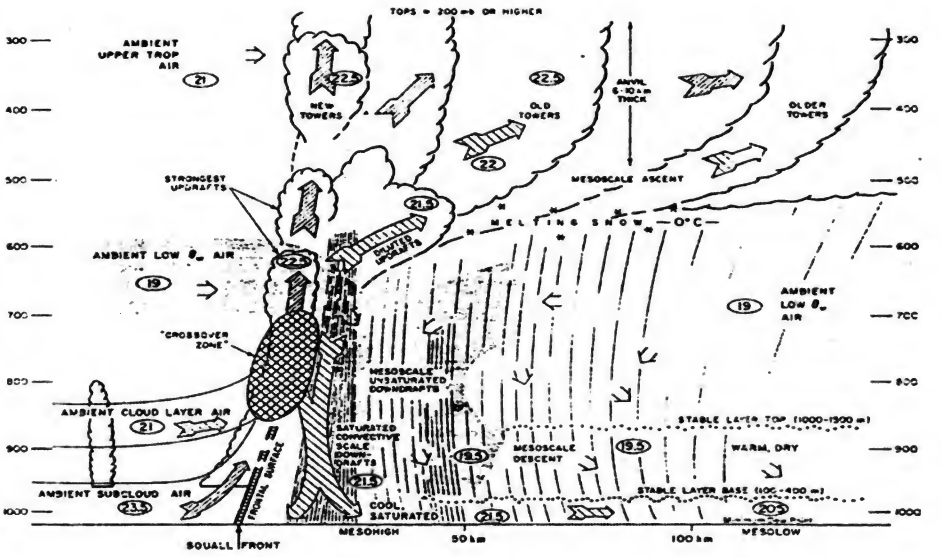

Figure 19: Schematic cross section through a class of mesoscale convective system. All flow is relative to the convective system.which is moving from right to left. Circled numbers are typical value of potential temperature in ^{o}C. It shows that parcels of sub-cloud boundary layer air rise and form the basic convective updrafts. Ambient cloud layer air is entrained into the updrafts. The updraft parcels rise till they lose their boundary by entrainment or by encountering a stable layer in the environment. Entrainment of ambient low equivalent-potential-temperature Air weakens updrafts and forms convective-scale downdrafts, which sink to the surface in the convective precipitation zone. Note that the system has three-dimensionality such that the updraft and downdraft trajectories are not collocated, and the convective region contains a "crossover zone" where convective-scale updrafts and downdrafts coexist. Adapted from Zipser (1977).

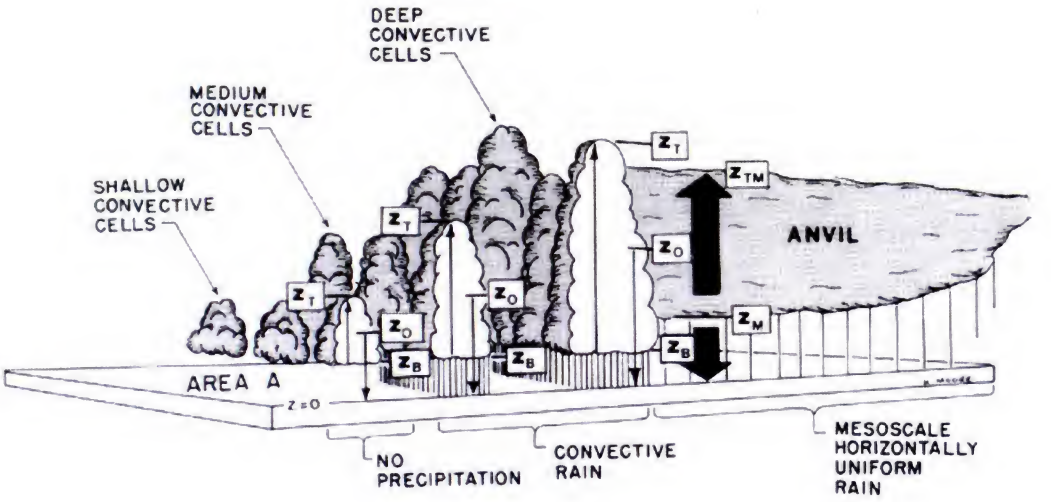

Figure 20: Schematic diagram of a typical population of clouds over a tropical ocean. Thi arrows represent convective-scale updrafts and downdrafts. Wide arrows represen mesoscale updrafts and downdrafts. Z_B and Z_T stand for cloud base and cloud top respectively. Z_M and Z_{TM} stand for the anvil's cloud base and cloud top, respectively. Z_o i the starting height of the downdrafts. It basically assumes that the cloud population contain convective cells ranging in size from shallow non-precipitating ceels to medium-size precipitating cells to deep precipitating cells. There is also a convective-scale updraft and convective-scale downdraft within each convective cell. Furthermore, the system has widespread anvil cloud which can deposit large quantities of horizontally uniform rain ove a mesoscale region. A mesoscale updraft can occur in the anvil, between level Z_M and Z_{TM} Adapted from Houze et al. (1980).

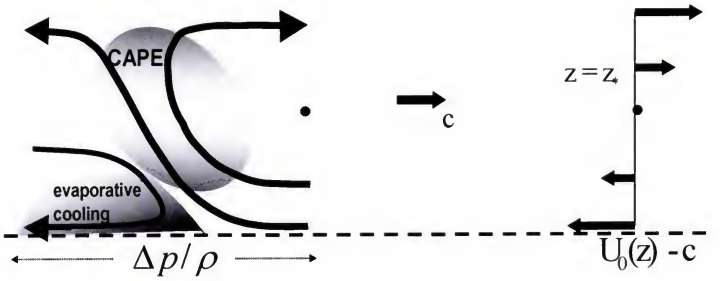

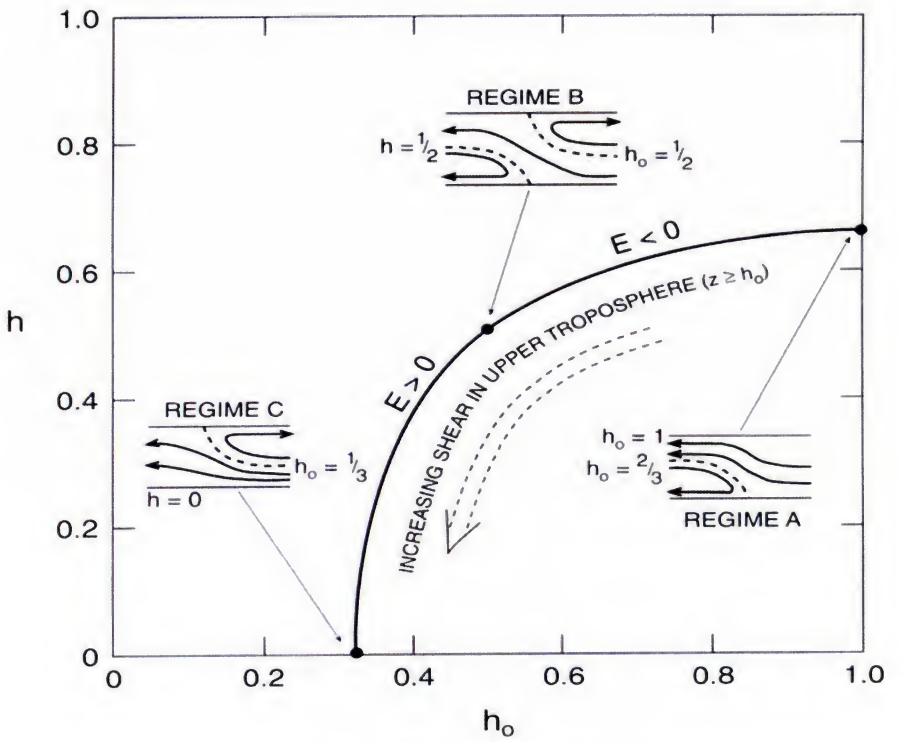

Figure 21: Upper, the 3-branch propagating convective organzation morphology showing the three types of available energy: CAPE, kinetic energy of inflow $\frac{1}{2}(U_0 - c)^2$ *and work done by pressure* $\Delta p/\rho$. *Lower, regimes of organization: propagating (A; E = -8/9), symmetric (B, E=0), hydraulic jump-like (C; E=1). [Courtesy: Moncrieff (1992).]*

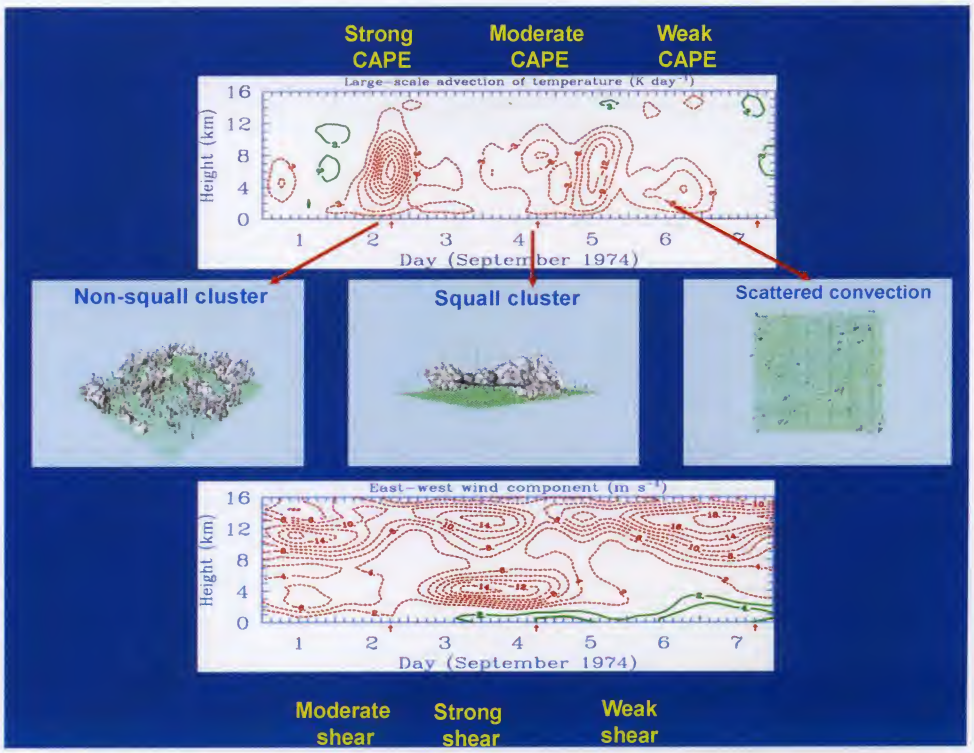

Figure 22: Three regimes organized precipitating convection simulated by a CRM: a) non-squall cluster for strong CAPE and moderate shear; b) squall cluster for moderate CAPE and strong shear; c) scattered convection for weak CAPE and weak shear. The squall cluster has the characteristic backward-tilted morphology of a squall line. [Courtey: Grabowski et al. 1998].

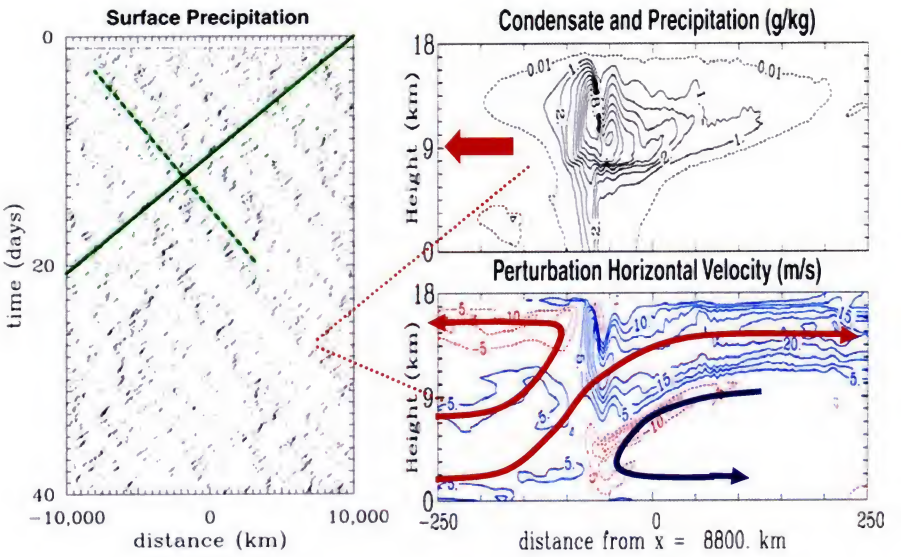

Figure 23: Multiscale convective organization in a two-dimensionalCRM with a 20,000 km domain: westward-propagating precipitating systems embedded in a eastward-propagating cloud-cluster envelopes. The vertical section shows the three-branch MCS-type airflow organization typical of the westward-moving systems. The multiscale organization developed from a randomly perturbed horizontally homogenous motionless state. [Grabowski and Moncrieff (2001)].

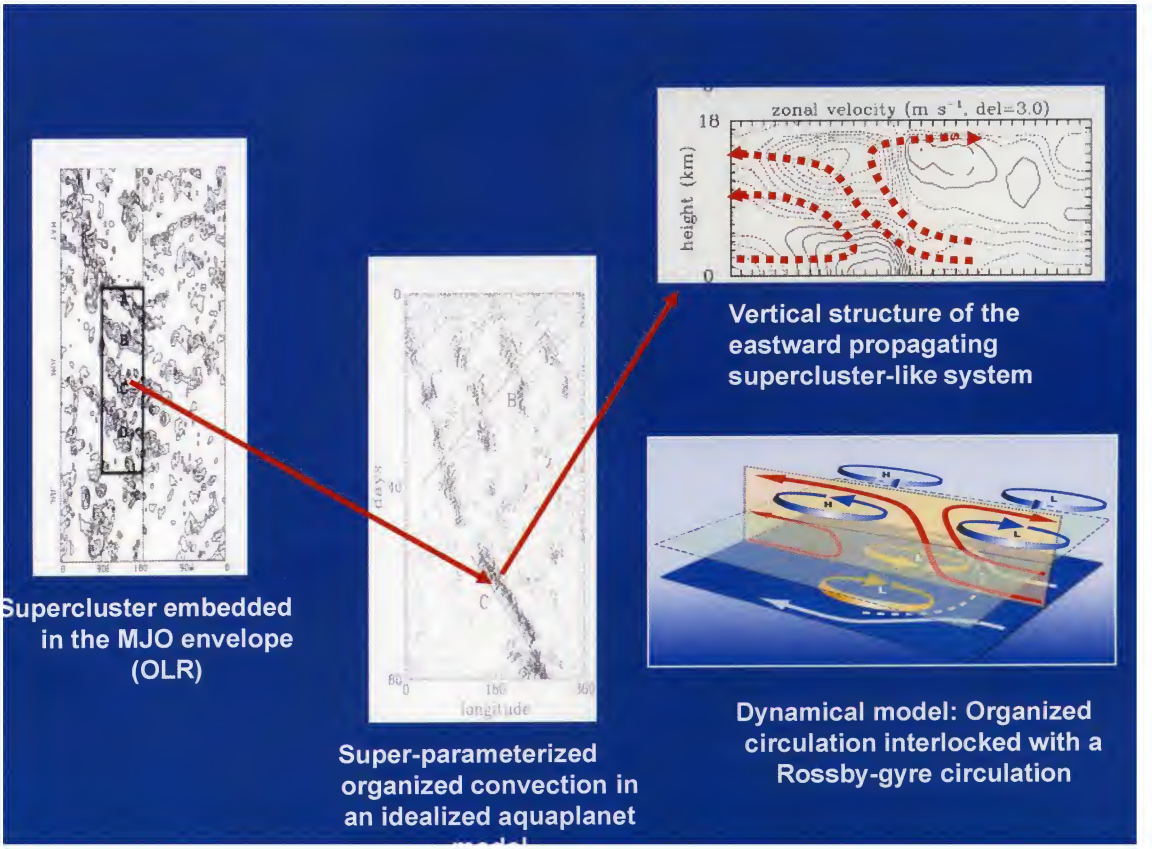
zonal velocity (m s⁻¹, del=3.0)
height (km)
18
0
Supercluster embedded in the MJO envelope (OLR)
Super-parameterized organized convection in an idealized aquaplanet
Vertical structure of the eastward propagating supercluster-like system
Dynamical model: Organized circulation interlocked with a Rossby-gyre circulation

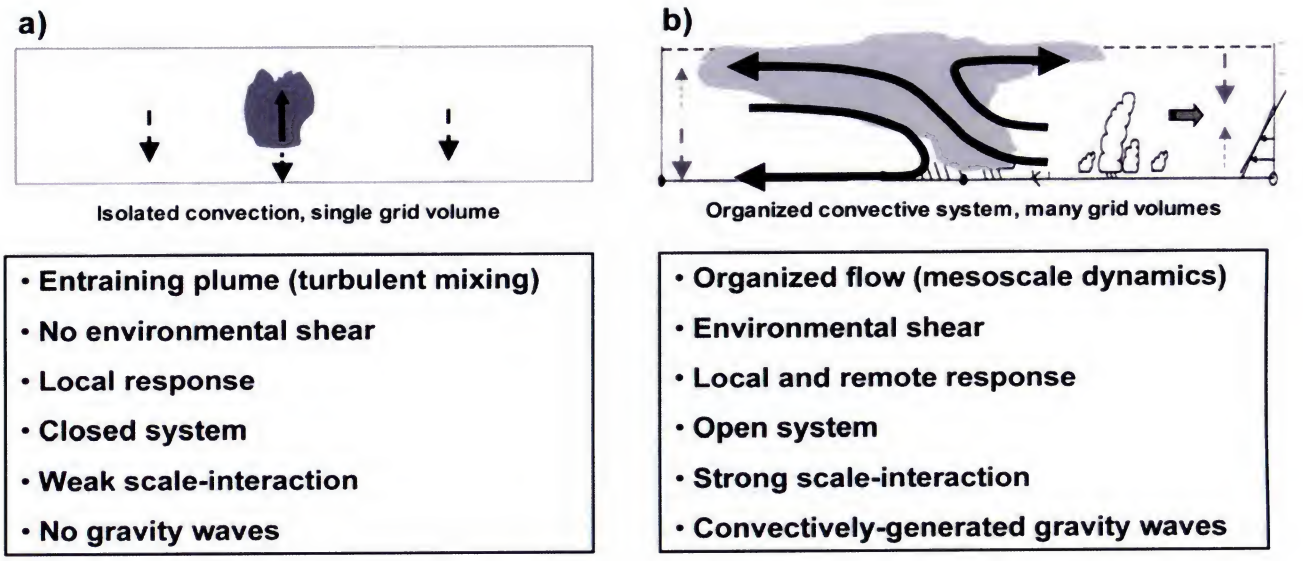

Figure 25: Distinction between: a) ordinary convection and b) organized convection. In the latter, the coherent flow and propagation evinces effects of vertical shear, far-field effects, and interaction with the large-scale flow. [Courtesy: Moncrieff and Liu (2006).]

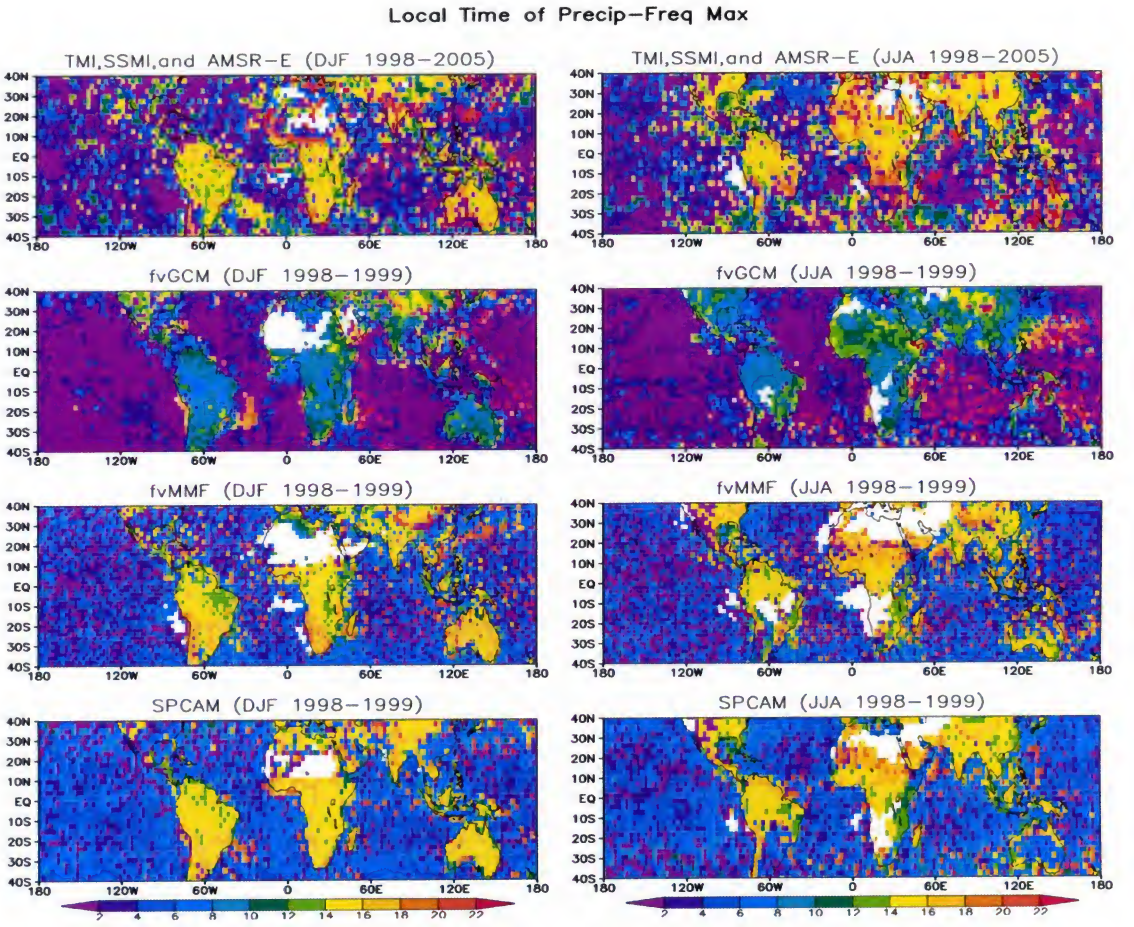

Figure 26: Geographical distribution of the local solar time (LST) for the non-drizzle precipitation frequency maximum in winter (left panels) and summer (right panels) as observed by satellite from 1998-2005 (upper panels) and as simulated for two years (1998-1999) with the Goddard fvGCM (middle-upper panels), Goddard MMF (middle-lower panels) and CSU MMF (bottom panels). Blank regions indicate no precipitation. The MMF results are based on detailed 2D GCE model-simulated hourly rainfall output. Satellite retrieved rainfall is based on a 5-satellite constellation including the TRMM Microwave Imager (TMI), Special Sensor Microwave Imager (SSMI) from the Defense Meteorological Satellite Program (DMSP) F13, F14 and F15, and the Advanced Microwave Scanning Radiometer – Earth Observing System (AMSR-E) onboard the Aqua satellite. The MMF-simulated diurnal variation of precipitation shows good agreement with merged microwave observations. For example, the MMF-simulated frequency maximum was in the late afternoon (1400-1800 LST) over land and in the early morning (0500-0700 LST) over the oceans. The fvGCM-simulated frequency maximum was too early for both oceans and land Adapted from Tao et al. (2008).